© 2010 Benjamin Robert Schudel

MICROFLUIDIC CHIPS FOR COMBINATORIAL SCREENING APPLICATIONS

BY

BENJAMIN ROBERT SCHUDEL

DISSERTATION

Submitted in partial fulfillment of the requirements
for the degree of Doctor of Philosophy in Chemical Engineering
in the Graduate College of the
University of Illinois at Urbana-Champaign, 2010

Urbana, Illinois

Doctoral Committee:

Associate Professor Paul J. A. Kenis, Chair
Professor Huimin Zhao
Associate Professor Brian T. Cunningham
Assistant Professor Charles M. Schroeder

Abstract

A wealth of small molecule compounds exist that may inhibit cancer or virus-causing diseases, and a wide array of experiments must be performed to narrow down the hundreds of thousands of possible candidates to a few biologically relevant compounds that could serve as ideal drug candidates. Microscale systems have the ability to duplicate benchtop screening experiments with the same fidelity at much smaller scales. Microscale experiments also have the benefit of using very little precious reagent, giving the economic value of low volume usage.

In order to develop high density microscale experimental combinatorics, a new valve was developed that is passively closed at rest, termed Actuate-to-Open (AtO) valves. Chapter 2 reports new design rules for AtO valve operation, both in single valve studies and in large on-chip arrays. The AtO valves are also employed in a combinatorial screening chip with a reversible seal that allows for interchangeable sensing capabilities. In Chapter 3, the combinatorial screening chip is integrated with a photonic crystal biosensor capable of screening for binding events in a label free fashion. A proof-of-principle protein-antibody assay was performed to validate the combinatorial features of the chip. In Chapter 4, the combinatorial chip was integrated with a molecular beacon patterned glass cover slip capable of detecting complimentary DNA fragments. Total internal reflection fluorescence (TIRF) microscopy is used for read out of the chip. Four virus-like oligomer targets with sequences corresponding to key fragments of the viruses HIV, HPV, Hepatitis A and Hepatitis B were tested against four different molecular beacons, each complementary to one of the four virus target oligonucleotides. The result of this combinatorial screening chip indicated strong fluorescent values for the matching beacon-target pairs, with statistically insignificant values for non-matching targets. This experiment not only established proof of principle of on-chip virus detection, it also demonstrated the high specificity of surface immobilized molecular beacons used in combination with TIRF.

Acknowledgements

I would like to thank Dr. Paul J. A. Kenis for his patience and guidance over the years of my doctoral thesis and for providing a thoughtful and engaging research environment for which to pursue this work. His scope and vision provided the backdrop for which this project propelled, and the collaborations he built allowed for me to expand the scope of this work into biological screening and microchemical insight.

I would also like to thank my collaborators on the combinatorial screening chip, namely Charles J. Choi, Ian Block and Dr. Brian T. Cunningham. Their insight into challenges that arose when combining our technologies helped move the project ever forward to the final state.

For the multiplex virus chip, I would like to thank Dr. Charles M. Schroeder for inviting me into his laboratory and allowing me to pontificate the virtues of latter day research assistantship to the young impressionable students of his lab, as well as Dr. Melikhan Tanyeri for vibrant discussion and passion within the work of fluorescence spectroscopy. I would also like to thank other members of his lab, including Christopher Brockman and Eric Johnson, for their assistance with microscope and lab usage.

And finally, I would like to thank the other members of the Kenis group lab. Sarah Perry provided excellent editorial and scientific assistance, with additional assistance from Fikile Brushett, Michael Thorson, Devin Whipple, and Adam Hollinger. For her valve studies work, Ritika Mohan gets due credit as well, and I wish her well on the challenges ahead in succeeding me on this project. Funding for this work was provided through the National Science Foundation, through the University of Illinois Nano-CEMMS Center.

for my parents,
who sacrificed quite a bit to get me here

Table of Contents

Chapter 1

Introduction

1.1. Background

Biological screening is an expensive and time-consuming process that is currently performed in a well plate format using microliters of material that can be difficult to come by in quantity for some systems. But these experiments performed at the benchtop scale could be repeated reliably at the microscale, using only picoliters of a reagent to yield the same results. In drug discovery or virus detection, using tiny amount of precious synthetic precursors or patient blood sample will reduce cost and easier experimental processes than their macroscale counterparts.

Downscaling an experiment often leads to reduced time and less cost. For example, a 4 inch x 3 inch well plate with 96 wells can consume 300 μL per well for a total of ~3 mL. These same reactions can be performed at the microfluidic scale, using picoliters of reagent per reaction in microfluidic devices. Even accounting for dead volume located within filling ports (~4 μL), typical X inch by y Inch microfluidic chips achieve the same chemistry using only a thousandths of the same material in a high throughput configuration. The same number of chemical reactions can be performed, just at smaller scales, which has the potential to save time, for example due to more

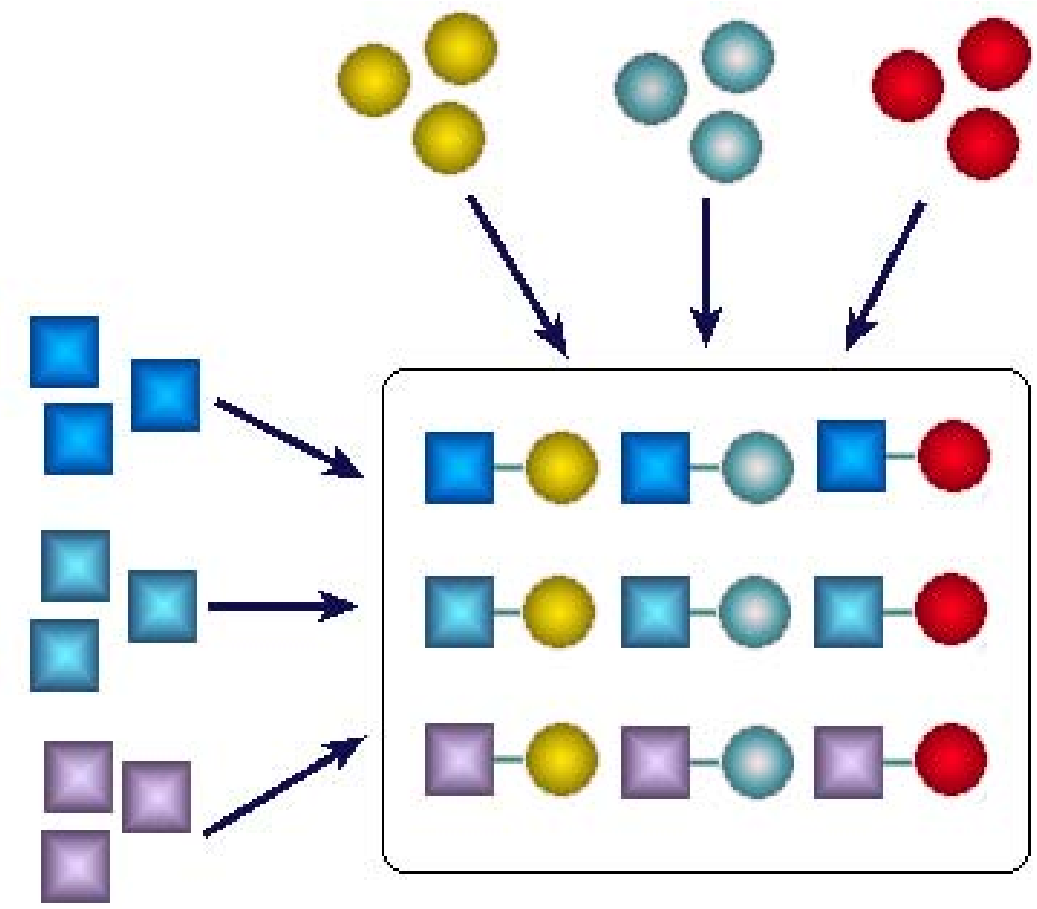

Figure 1.1. A schematic of a combinatorial screening technique on a well plate. In this scheme, six reactants combine in a combinatorial fashion to develop nine separate and distinct products. For precious reagents, reducing the volumes of the individual reactants becomes tantamount.

efficient mixing. When experiments become prohibitively costly or time-intensive, a microfluidic route reduces both the effort and expense.

The physical and chemical phenomena that occur at these surface-force dominated regions can also be exploited to maximum benefit within microfluidic chips. The low Reynolds number and high surface-to-volume ratios that occur within microfluidic systems can be exploited for excellent control over mass and heat transport phenomena. For example, by shrinking the scale at which experimental procedures are

performed, a new level of control can be imposed on the mixing of reagents to produce higher yields [1-6] or finer temperature control [7-13]. These advantages have been explored in, for example, chemical synthesis [14-20], PCR amplification [21-28], and electrochemical systems [29-36].

In terms of screening, where large arrays of compounds are tested against sensors using as little material as possible per screening event, microfluidic devices can serve as a huge advantage to performing high fidelity experiments. This thesis will cover the implementation of a new passively closed valve, termed here as Actuate-to-Open (AtO) valves. These valves enable highly portable, large scale high-density combinatorial devices that can be implemented in possible drug screening chips or virus screening.

1.2. Screening at the Microscale

Microfluidic devices provide for excellent control of very small volumes, however analysis of the volumes at the sub-nanoliter scale can become exceedingly difficult. Traditional IR or UV/Vis techniques are not suitable, due to the very small path length through droplets that are typically compressed to 10 micrometers in height. Because these volumes are so small, the signal to noise ratios gathered from such small volumes become insufficient for the detection of events such as molecular binding interactions. Recent advances in waveguide fabrication show some improvement in signal to noise ratio, but their fabrication requires intensive micromachining techniques [37-41].

In effect, utilizing bulk measurements becomes increasingly difficult when the volume in question decreases to a few microliters. While a microplate reader can

efficiently scan hundreds of microliter-sized wells per minute, the results from these experiments often focus on fluorescent proteins, such as green fluorescent protein (GFP) [42-47]. While not a problem for GFP due to the ease of production, when reagent becomes precious or fluorescent readout is not available, this type of microplate reader is unfortunately ineffective. For experiments with nanoliter or sub-nanoliter volumes, analysis must be done using surface-based techniques that can leverage high signal to noise ratios while ignoring volume sizes. This naturally leads to integration of surface-based biosensing techniques in a microfluidic environment.

Due to the sheer number of possible compounds for an average inhibition screen, parameter space can quickly become unmanageable. One method of variable simplification involves grouping similar compounds by family based on a defined reaction scheme, building so-called molecular libraries. These libraries are subsequently screened for interactions, or binding events with proteins to determine potential drug candidates in inhibition screens, with analysis by colorimetric or fluorescent readout [48-52]. A single protein might be tested against an array of compounds, as not all proteins are active at the same pH or salt conditions. These limitations lead toward an experimental setup that is scaled out rather than up, to cover the vast number of reactions on different chips in smaller wells without losing the accuracy observed in bench top experiments at the macroscale.

High throughput screening (HTS) is defined as performing a vast array of experiments using as little reagent as possible per experiment. One microscale example utilizes aqueous droplets suspended in oil that form due to the surface tension between both liquids [53-58]. Protein crystallization has been studied with hundreds of

aqueous droplets in such two-phase systems but may still only produce a few droplets with crystals viable for subsequent crystallography [59-63]. Other sensing techniques include MALDI [64-68], gas chromatography [69-72], and cytometry for microliter-scale systems [73-76]. Fluorescence based assays in particular have been utilized in screening experiments [77], detection of toxins [78-80] and cell proliferation studies [81, 82].

While vast in their application, these screening techniques are limited to the number of variables that can be examined within each experiment on a chip, particularly the different compounds that each droplet contains. Single layer microfluidic chips depend on oil-water emulsions to produce separation from experiment to experiment. Although assays have been performed in thousands of droplets looking at few variables [82, 83], synthesizing molecular libraries on a chip is not feasible with this technique. Microscale chips analogous to 96-well plate experiments are few, and an elegant method of mixing large numbers of nanoliters droplets in a controlled way has still not been evaluated.

Recent advances in click chemistry have yielded a host of relevant heterocyclic small molecules [18, 52, 84]. "Click chemistry" is so termed because the bimolecular reactions of relatively unstable reactants 'click' into place to create new heterocyclic small molecules capable of binding to disease related proteins. While the final bimolecular reactions are easily done in water with copper catalyst, the precursor molecules can be quite difficult to synthesize, with poor yields [84-86].

1.3. Microfluidic Approaches

Multilayer soft lithography (MSL) is a technique developed by Quake *et al.* for rapidly fabricating sophisticated microfluidic chips with integrated valves that can be

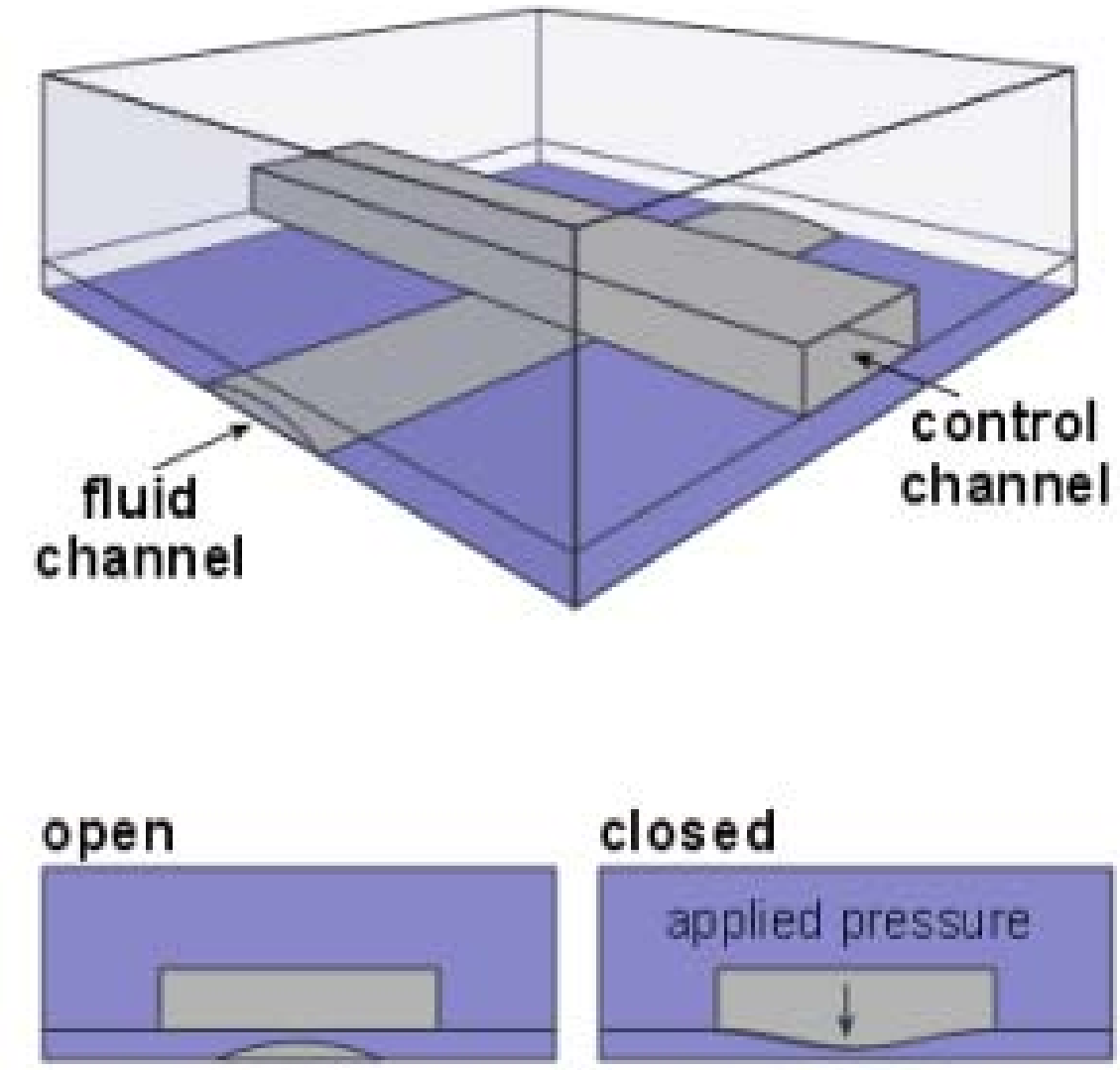

Figure 1.2. A schematic of actuate-to-close (AtC) valves fabricated using multilayer soft lithography (MSL). A microchannel in a control layer is fabricated in PDMS and aligned over a microchannel in a thin fluid layer. The valves are open in the rest state (open), and collapse shut on the application of an external pressure (closed).

used to control separation and mixing at the microscale [87-91]. Two different layers are replicated in polydimethylsiloxane (PDMS) using soft lithography: a fluidic layer composed of microchannels designed to house the necessary liquid reagents, and a control layer containing actuate-to-close (AtC) valves. This second layer is placed on top of the fluid layer so fluid flow can be controlled in the underlying fluid layer (Figure 1.2). This multilayer microfluidic chip configuration has been demonstrated to vastly increase control at the microscale. This has been employed in a wide range of applications, including rotary pumps [88], cell sorting [89, 92], cell culture [92, 93], and optofluidics [94-97]. The distinct advantages to using MSL in microfluidic chips is the ability to isolate portions of a microchannel and being able to control fluidic movement within the confines of nano- or pico- liter-sized reactors to perform experiments that were not feasible on the macroscale.

Some difficulties arise when employing the technique of MSL for making actuate-to-close valves. For example, an irreversible seal is required between all layers of the chip, due to of the fact that positive pressure is used in the valves of the control layer and the channels of the fluid layer to capture and move fluid plugs. Because the valves are passively open, the chip must be externally linked to pressure-controlled ancillaries for the duration of the experiment. This is not a problem when readout is integrated into the chamber but can become taxing when the chip must be transported for screening.

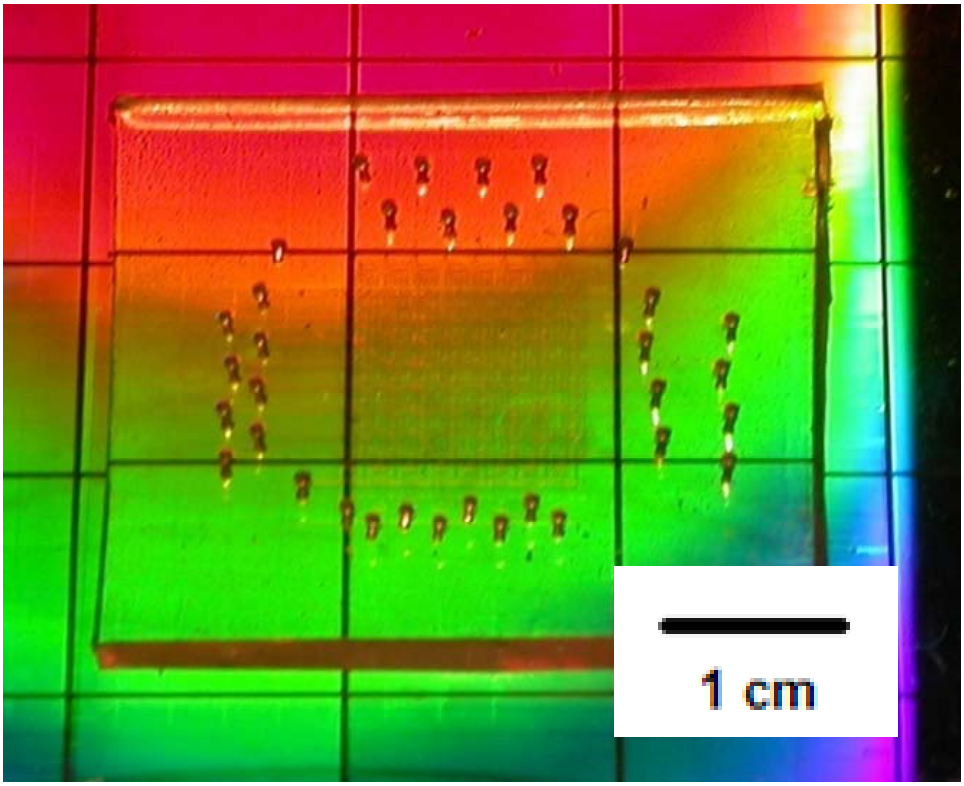

Figure 1.3. A microfluidic combinatorial chip integrated to an unpatterned photonic crystal biosensor. This chip is capable of 8x8 reactions for a total of 64 products formed from 16 reagents.

1.4. Combinatorial Microfluidic Screening

We have used MSL to design and study actuate-to-open (AtO) valves, valves that are closed in rest, that overcome many issues associated with the use of microfluidic chips with AtC valves. The integration of new AtO valves allows microfluidic chips to be decoupled from ancillaries and thus to be freely transported post-filling, such as the combinatorial chip shown in Figure 1.3. The design, fabrication, and characterization of these AtO valves will be described in Chapter 2. Microfluidic chips based on these passively closed valves will be employed in combinatorial mixing chips capable of two types of on-chip screening. A non-fluorescence based system

employing a photonic crystal biosensor for screening combinatorial products against cancer-related proteins will be discussed in Chapter 3. Then, in Chapter 4 a fluorescence-based approach that is suitable for screening of viral compounds within a microfluidic well plate will be discussed. Chapter 5 will summarize the results described in this thesis, and provide an outlook with respect to the utility of AtO valves, and microfluidic chips that use them, as well as applications of such chips.

1.5. References

1. Klavs F. Jensen, *Microchemical systems: Status, challenges, and opportunities.* AIChE Journal, 1999. **45**(10): p. 2051-2054.
2. Pelter, M.W., L.S.W. Pelter, D. Colovic, and R. Strug, *Microscale Synthesis of 1-Bromoe-3-chloro-5-iodobenzene: An Improved Deamination of 4-Bromo-2-chloro-5-iodoaniline.* Journal of Chemical Education, 2004. **81**(1): p. 111-112.
3. Li, D.Y., L. Wang, and W. Li, *Effects of grain size from micro scale to nanoscales on the yield strain of brass under compressive and tensile stresses using a Kelvin probing technique.* Materials Science and Engineering A, 2004. **384**(1-2): p. 355-360.
4. Agrawal, N. and A. Kohen, *Microscale synthesis of 2-tritiated isopropanol and 4R-tritiated reduced nicrotinamide adenine dinucleotide phosphate.* Analytical Biochemistry, 2003. **322**: p. 179-184.
5. Ronneberg, A., G. Metz, R. Weld, P. Roffey, and C. Craney, *A high yield microscale enzymatic synthesis and purification Of C-Labeled Nicotinamide Adenine Dinucleotide Phosphate.* Journal of Labelled Compounds and Radiopharmaceuticals, 1992. **31**(4): p. 329-332.
6. Song, X., Y. Lasanajak, B. Xia, D.F. Smith, and R.D. Cummings, *Fluorescent Glycosylamides Produced by Microscale Derivatization of Free Glycans for Natural Glycan Microarrays.* ACS Chemical Biology, 2009. **4**(9): p. 741-750.
7. Erickson, D., D. Sinton, and D. Li, *Joule heating and heat transfer in poly(dimethylsiloxane) microfluidic systems.* Lab on a Chip, 2003. **3**: p. 141-149.
8. Höhmann, C. and P. Stephan, *Microscale temperature measurement at an evaporating liquid meniscus.* Experimental Thermal and Fluid Science, 2002. **26**(2-4): p. 157-162.
9. Slyadnev, M.N., Y. Tanaka, M. Tokeshi, and T. Kitamori, *Photothermal Temperature Control of a Chemical Reaction on a Microchip Using an Infrared Diode Laser.* Analytical Chemistry, 2001. **73**(16): p. 4037-4044.
10. Yoon, D.S., Y.-S. Lee, Y. Lee, H.J. Cho, S.W. Sung, K.W. Oh, J. Cha, and G. Lim, *Precise temperature control and rapid thermal cycling in a micromachined DNA polymerase chain reaction chip.* Journal of Micromechanics and Microengineering, 2002. **12**: p. 813.
11. Tanaka, Y., M.N. Slyadnev, A. Hibara, M. Tokeshi, and T. Kitamori, *Non-contact photothermal control of enzyme reactions on a microchip by using a compact diode laser.* Journal of Chromatography A, 2000. **894**(1-2): p. 45-51.
12. Easley, C.J., L.A. Legendre, M.G. Roper, T.A. Wavering, J.P. Ferrance, and J.P. Landers, *Extrinsic Fabryâˆ'Perot Interferometry for Noncontact Temperature*

Control of Nanoliter-Volume Enzymatic Reactions in Glass Microchips. Analytical Chemistry, 2005. **77**(4): p. 1038-1045.

13. Guijt, R.M., A. Dodge, G.W.K. van dedem, N.F. de Rooij, and E. Verpoorte, *Chemical and physical processes for integrated temperature control in microfluidic devices.* Lab on a Chip, 2002. **3**: p. 1-4.
14. Miyazaki, M., H. Nakamura, and H. Maeda, *Improved yield of enzyme reaction in microchannel reactor.* Chemistry Letters, 2001. **30**(5): p. 442-443.
15. Nie, Z., W. Li, M. Seo, S. Xu, and E. Kumacheva, *Janus and Ternary Particles Generated by Microfluidic Synthesis:â€‰ Design, Synthesis, and Self-Assembly.* Journal of the American Chemical Society, 2006. **128**(29): p. 9408-9412.
16. Chan, E.M., A.P. Alivisatos, and R.A. Mathies, *High-Temperature Microfluidic Synthesis of CdSe Nanocrystals in Nanoliter Droplets.* Journal of the American Chemical Society, 2005. **127**(40): p. 13854-13861.
17. Chan, E.M., R.A. Mathies, and A.P. Alivisatos, *Size-Controlled Growth of CdSe Nanocrystals in Microfluidic Reactors.* Nano Letters, 2003. **3**(2): p. 199-201.
18. Lewis, P.C., R.R. Graham, Z. Nie, S. Xu, M. Seo, and E. Kumacheva, *Continuous Synthesis of Copolymer Particles in Microfluidic Reactors.* Macromolecules, 2005. **38**(10): p. 4536-4538.
19. Khan, S.A., A. Gunther, M.A. Schmidt, and K.F. Jensen, *Microfluidic synthesis of colloidal silica.* Langmuir, 2004. **20**(20): p. 8604-8611.
20. Shepherd, R.F., J.C. Conrad, S.K. Rhodes, D.R. Link, M. Marquez, D.A. Weitz, and J.A. Lewis, *Microfluidic Assembly of Homogeneous and Janus Colloid-Filled Hydrogel Granules.* Langmuir, 2006. **22**(21): p. 8618-8622.
21. Zhang, C., J. Xu, W. Ma, and W. Zheng, *PCR microfluidic devices for DNA amplification.* Biotechnology Advances. **24**(3): p. 243-284.
22. Khandurina, J., T.E. McKnight, S.C. Jacobson, L.C. Waters, R.S. Foote, and J.M. Ramsey, *Integrated System for Rapid PCR-Based DNA Analysis in Microfluidic Devices.* Anal. Chem., 2000. **72**: p. 2995-3000.
23. Lagally, E.T., P.C. Simpson, and R.A. Mathies, *Monolithic integrated microfluidic DNA amplification and capillary electrophoresis analysis system.* Sensors and Actuators B: Chemical, 2000. **63**(3): p. 138-146.
24. Khandurina, J., T.E. McKnight, S.C. Jacobson, L.C. Waters, R.S. Foote, and J.M. Ramsey, *Integrated System for Rapid PCR-Based DNA Analysis in Microfluidic Devices.* Analytical Chemistry, 2000. **72**(13): p. 2995-3000.
25. Lagally, E.T., I. Medintz, and R.A. Mathies, *Single-Molecule DNA Amplification and Analysis in an Integrated Microfluidic Device.* Analytical Chemistry, 2001. **73**(3): p. 565-570.

26. Kamei, T., N.M. Toriello, E.T. Lagally, R.G. Blazej, J.R. Scherer, R.A. Street, and R.A. Mathies, *Microfluidic Genetic ANalysis with an Integrated a-Si:H Detector.* Biomedical Microdevices, 2005. **7**(2): p. 147-152.

27. Pilarski, L.M., J. Lauzon, E. Strachan, S. Adamia, A. Atrazhev, A.R. Belch, and C.J. Backhouse, *Sensitive detection using microfluidics technology of single cell PCR products from high and low abundance IgH VDJ templates in multiple myeloma.* Journal of Immunological Methods, 2005. **305**(1): p. 94-105.

28. Nelson, R.J., H.H. Hooper, A.K. KHauser, S. Singh, S.J. Williams, and A.P. Sassi, *Microfluidic Method for Nucleic Acid Purification and Processing*, U.S.P. Office, Editor. Aug 29, 2002, ACLARA Biosciences, Inc.: USA.

29. Choban, E.R., L.J. Markoski, A. Wieckowski, and P.J.A. Kenis, *Microfluidic fuel cell based on laminar flow.* Journal of Power Sources, 2004. **128**(1): p. 54-60.

30. Lin, Y., C.A. Timchalk, D.W. Matson, H. Wu, and K.D. Thrall, *Integrated Microfluidics/Electrochemical Sensor System for Monitoringof Environmental Exposures to Lead and Chlorophenols.* Biomedical Microdevices, 2001. **3**(4): p. 331-338.

31. Yoon, S.K., G.W. Fichtl, and P.J.A. Kenis, *Active control of the depletion boundary layers in microfluidic electrochemical reactors.* Lab on a Chip, 2006. **6**: p. 1516-1524.

32. Pavlovic, E., R.Y. Lai, L.T. Wu, B.S. Ferguson, R. Sun, K.W. Plaxco, and H.T. Soh, *Microfluidic Device Architecture for Electrochemical Patterning and Detection of Multiple DNA Sequences.* Langmuir, 2008. **24**(3): p. 1102-1107.

33. Zhan, W. and R.M. Crooks, *Microelectrochemical Logic Circuits.* Journal of the American Chemical Society, 2003. **125**(33): p. 9934-9935.

34. Rossier, J., F. Reymond, and P.E. Michel, *Polymer microfluidic chips for electrochemical and biochemical analyses.* Electrophoresis, 2002. **23**(6): p. 858-867.

35. Swensen, J.S., Y. Xiao, B.S. Ferguson, A.A. Lubin, R.Y. Lai, A.J. Heeger, K.W. Plaxco, and H.T. Soh, *Continuous, Real-Time Monitoring of Cocaine in Undiluted Blood Serum via a Microfluidic, Electrochemical Aptamer-Based Sensor.* Journal of the American Chemical Society, 2009. **131**(12): p. 4262-4266.

36. Choi, J.-W., K.W. Oh, J.H. Thomas, W.R. Heineman, H.B. Halsall, J.H. Nevin, A.J. Helmicki, T. Henderson, and C.H. Ahn, *An integrated microfulidic biochemical detection system for protein analysis with magnetic bead-based sampling capabilities.* Lab on a Chip, 2001. **2**: p. 27-30.

37. Petersen, N.J., K.B. Mogensen, and J.P. Kutter, *Performance of an in-plane detection cell with integrated waveguides for UV/Vis absorbance measurements on microfluidic separation devices.* Electrophoresis, 2002. **23**: p. 3528-3536.

38. Vezenov, D.V., B.T. Mayers, R.S. Conroy, G.M. Whitesides, P.T. Snee, Y. Chan, D.G. Nocera, and M.G. Bawendi, *A Low-Threshold, High-Efficiency Microfluidic*

Waveguide Laser. Journal of the American Chemical Society, 2005. **127**(25): p. 8952-8953.

39. Sun, H., F. He, Z. Zhou, Y. Cheng, Z. Xu, K. Sugioka, and K. Midorikawa, *Fabrication of microfluidic optical waveguides on glass chips with femtosecond laser pulses.* Opt. Lett., 2007. **32**: p. 1536-1538.

40. Psaltis, D., S.R. Quake, and C. Yang, *Developing optofluidic technology through the fusion of microfluidics and optics.* Nature, 2006. **442**(7101): p. 381-386.

41. Whitesides, G.M., *The origins and the future of microfluidics.* Nature, 2006. **442**(7101): p. 368-373.

42. Lorenzen, A. and S.W. Kennedy, *A Fluorescence-Based Protein Assay for Use with a Microplate Reader.* Analytical Biochemistry, 1993. **214**(1): p. 346-348.

43. Chalfie, M., Y. Tu, G. Euskirchen, W.W. Ward, and D.C. Prasher, *Green fluorescent protein as a marker for gene expression.* Science, 1994. **263**(5148): p. 802-805.

44. Kassack, M.U., B. Hofgen, J. Lehmann, N. Eckstein, J.M. Quillan, and W. Sadee, *Functional Screening of G Protein--Coupled Receptors by Measuring Intracellular Calcium with a Fluorescence Microplate Reader.* J Biomol Screen, 2002. **7**(3): p. 233-246.

45. Huang, D., B. Ou, M. Hampsch-Woodill, J.A. Flanagan, and R.L. Prior, *High-Throughput Assay of Oxygen Radical Absorbance Capacity (ORAC) Using a Multichannel Liquid Handling System Coupled with a Microplate Fluorescence Reader in 96-Well Format.* Journal of Agricultural and Food Chemistry, 2002. **50**(16): p. 4437-4444.

46. Glenny, R.W., S. Bernard, and M. Brinkley, *Validation of fluorescent-labeled microspheres for measurement of regional organ perfusion.* J Appl Physiol, 1993. **74**(5): p. 2585-2597.

47. Nakatsubo, N., H. Kojima, K. Kikuchi, H. Nagoshi, Y. Hirata, D. Maeda, Y. Imai, T. Irimura, and T. Nagano, *Direct evidence of nitric oxide production from bovine aortic endothelial cells using new fluorescence indicators: diaminofluoresceins.* FEBS Letters, 1998. **427**(2): p. 263-266.

48. MacBeath, G., *Protein microarrays and proteomics.* Nat Genet.

49. de Silva, P.A., N.H.Q. Gunaratne, and C.P. McCoy, *A molecular photoionic AND gate based on fluorescent signalling.* Nature, 1993. **364**(6432): p. 42-44.

50. Dauwerse, J.G., J. Wiegant, A.K. Raap, M.H. Breuning, and G.J.B. van Ommen, *Multiple colors by fluorescence in situ hybridization using ratio-labelled DNA probes create a molecular karyotype.* Hum. Mol. Genet., 1992. **1**(8): p. 593-598.

51. Kerppola, T.K., *Visualization of molecular interactions by fluorescence complementation.* Nat Rev Mol Cell Biol, 2006. **7**(6): p. 449-456.

52. Solinas, R., J.C. DiCesare, and P.W. Baures, *Parallel Synthesis of an Imidazole-4,5-dicarboxamide Library Bearing Amino Acid Esters and Alkanamines.* Molecules, 2008. **13**(12): p. 3149-3170.

53. Olsen, M., B. Iverson, and G. Georgiou, *High-throughput screening of enzyme libraries.* Current Opinion in Structural Biology, 2000. **11**: p. 331-337.

54. Anna, S.L., N. Bontoux, and H.A. Stone, *Formation of dispersions using "flow focusing" in microchannels.* Applied Physics Letters, 2003. **82**: p. 1537519.

55. Kawakatsu, T., H. Komori, M. Nakajima, Y. Kikuchi, and T. Yonemoto, *Production of Monodispersed Oil-in-Water Emulsion Using Crossflow-Type Silicon Microchannel Plate.* Journal of Chemical Engineering of Japan, 1999. **32**(2): p. 241-244.

56. Kawakatsu, T., G. Trägårdh, C. Trägårdh, M. Nakajima, N. Oda, and T. Yonemoto, *The effect of the hydrophobicity of microchannels and components in water and oil phases on droplet formation in microchannel water-in-oil emulsification.* Colloids and Surfaces A: Physicochemical and Engineering Aspects, 2001. **179**(1): p. 29-37.

57. Ueno, K., F. Kitagawa, and N. Kitamura, *Photocyanation of pyrene across an oil/water interface in a polymer microchannel chip.* Lab on a Chip, 2002. **2**: p. 231-234.

58. Nisisako, T., T. Torii, and T. Higuchi, *Droplet formation in a microchannel network.* Lab on a Chip, 2002. **2**: p. 24-26.

59. Zheng, B., L.S. Roach, and R.F. Ismagilov, *Screening of Protein Crystallization Conditions on a Microfluidic Chip Using Nanoliter-Sized Droplets.* JACS, 2003. **125**: p. 11170-11171.

60. Perry, S.L., G.W. Roberts, J.D. Tice, R.B. Gennis, and P.J.A. Kenis, *Microfluidic Generation of Lipidic Mesophases for Membrane Protein Crystallization.* Crystal Growth & Design, 2009. **9**(6): p. 2566-2569.

61. Dittrich, P.S. and A. Manz, *Lab-on-a-chip: microfluidics in drug discovery.* Nat Rev Drug Discov, 2006. **5**(3): p. 210-218.

62. DeLucas, L.J., D. Hamrick, L. Cosenza, L. Nagy, D. McCombs, T. Bray, A. Chait, B. Stoops, A. Belgovskiy, W. William Wilson, M. Parham, and N. Chernov, *Protein crystallization: virtual screening and optimization.* Progress in Biophysics and Molecular Biology, 2005. **88**(3): p. 285-309.

63. William Wilson, W., *Light scattering as a diagnostic for protein crystal growth--A practical approach.* Journal of Structural Biology, 2003. **142**(1): p. 56-65.

64. Winkle, R.F., J.M. Nagy, A.E.G. Cass, and S. Sharma, *Towards microfluidic technology-based MALDI-MS platforms for drug discovery: a review.* Expert Opinion on Drug Discovery, 2008. **3**(11): p. 1281-1292.

65. Liu, J., K. Tseng, B. Garcia, C.B. Lebrilla, E. Mukerjee, S. Collins, and R. Smith, *Electrophoresis Separation in Open Microchannels. A Method for Coupling Electrophoresis with MALDI-MS.* Analytical Chemistry, 2001. **73**(9): p. 2147-2151.

66. Westman, A., G. Brinkmalm, and D.F. Barofsky, *MALDI induced saturation effects in chevron microchannel plate detectors.* International Journal of Mass Spectrometry and Ion Processes, 1997. **169-170**: p. 79-87.

67. Brivio, M., R.H. Fokkens, W. Verboom, D.N. Reinhoudt, N.R. Tas, M. Goedbloed, and A. van den Berg, *Integrated Microfluidic System Enabling (Bio)chemical Reactions with On-Line MALDI-TOF Mass Spectrometry.* Analytical Chemistry, 2002. **74**(16): p. 3972-3976.

68. Brivio, M., N.R. Tas, M. Goedbloed, H.J.G.E. Gardeniers, W. Verboom, A. Van den Berg, and D.N. Reinhoudt, *A MALDI-chip integrated system with a monitoring window.* Lab on a Chip, 2005. **5**: p. 378-381.

69. Shi, G., F. Hong, Q. Liang, H. Fang, S. Nelson, and S.G. Weber, *Capillary-Based, Serial-Loading, Parallel Microreactor for Catalyst Screening.* Analytical Chemistry, 2006. **78**(6): p. 1972-1979.

70. Kutter, J.P., *Current developments in electrophoretic and chromatographic separation methods on microfabricated devices.* TrAC Trends in Analytical Chemistry, 2000. **19**(6): p. 352-363.

71. Erikson, D. and D. Li, *Integrated microfluidic devices.* Analytica Chimica Acta, 2004. **507**: p. 11-26.

72. Gravesen, P. and et al., *Microfluidics-a review.* Journal of Micromechanics and Microengineering, 1993. **3**(4): p. 168.

73. McKenna, B.K., A.A. Selim, F.R. Bringhurst, and D.J. Ehrlich, *384-Channel parallel microfluidic cytometer for rare-cell screening.* Lab on a Chip, 2009. **9**(2): p. 305-310.

74. Yi, C., C.-W. Li, S. Ji, and M. Yang, *Microfluidics technology for manipulation and analysis of biological cells.* Analytica Chimica Acta, 2006. **560**(1-2): p. 1-23.

75. Huh, D. and et al., *Microfluidics for flow cytometric analysis of cells and particles.* Physiological Measurement, 2005. **26**(3): p. R73.

76. Wu, H., A. Wheeler, and R.N. Zare, *Chemical cytometry on a picoliter-scale integrated microfluidic chip.* Proceedings of the National Academy of Sciences of the United States of America, 2004. **101**(35): p. 12809-12813.

77. Darain, F., P. Yager, K.L. Gan, and S.C. Tjin, *On-chip detection of myoglobin based on fluorescence.* Biosensors and Bioelectronics.

78. Meagher, R.J., A.V. Hatch, R.F. Renzi, and A.K. Singh, *An integrated microfluidic platform for sensitive and rapid detection of biological toxins.* Lab on a Chip, 2008. **8**(12): p. 2046-2053.

79. Frisk, M.L., E. Berthier, W.H. Tepp, E.A. Johnson, and D.J. Beebe, *Bead-based microfluidic toxin sensor integrating evaporative signal amplification.* Lab on a Chip, 2008. **8**(11): p. 1793-1800.

80. Garcia-Alonso, J., G.M. Greenway, J.D. Hardege, and S.J. Haswell. *A prototype microfluidic chip using fluorescent yeast for detection of toxic compounds*. 2009: Elsevier Advanced Technology.

81. Schmitz, C.H.J., A.C. Rowat, S. Koster, and D.A. Weitz, *Dropspots: a picoliter array in a microfluidic device.* Lab on a Chip, 2009. **9**: p. 44-49.

82. Sia, S.K. and G.M. Whitesides, *Microfluidic devices fabrication in poly(dimethylsiloxane) for biological studies.* Electrophoresis, 2003. **24**(3563-3576).

83. Tice, J.D., H. Song, A.D. Lyon, and R.F. Ismagilov, *Langmuir.* Formation of Droplets and Mixing in Multiphase Microfluidics at Low Values of the Reynolds and the Capillary Numbers, 2003. **19**: p. 9127-9133.

84. Kolb, H.C., M.G. Finn, and K.B. Sharpless, *Click Chemistry: Diverse Chemical Function from a Few Good Reactions.* Angewandte Chemie International Edition, 2001. **40**(11): p. 2004-2021.

85. Tornoe, C.W., C. Christensen, and M. Meildal, *Peptiodotriazoles on Solid Phase: [1,2,3]-Triazoles by Regiospecific Copper(I)-Catalyzed 1,3-Dipolar Cycloadditions of Terminal Alkynes to Azides.* Journal of Organic Chemistry, 2002. **67**(9): p. 3057-3064.

86. Kolb, H.C. and K.B. Sharpless, *The growing impact of click chemistry on drug discovery.* Drug Discovery Today, 2003. **8**(24): p. 1128-1137.

87. Unger, M.A., H.-P. Chou, T. Thorsen, A. Scherer, and S.R. Quake, *Monolithic Microfabricated Valves and Pumps by Multilayer Soft Lithography.* Science, 2000. **288**(5463): p. 113-116.

88. Chou, H.-P., M.A. Unger, and S.R. Quake, *A Microfabricated Rotary Pump.* Biomedical Microdevices, 2001. **3**(4): p. 323-330.

89. Fu, A.Y., H.-P. Chou, C. Spence, F.H. Arnold, and S.R. Quake, *An Integrated Microfabricated Cell Sorter.* Anal. Chem., 2002. **74**: p. 2451-2457.

90. Liu, J., C. Hansen, and S.R. Quake, *Solving the "World-to-Chip" Interface Problem with a Microfluidic Matrix.* Anal. Chem., 2003. **75**: p. 4718-4723.

91. Thorsen, T., S.J. Maerkl, and S.R. Quake, *Monolithic Microfabricated Valves and Pumps by Multilayer Soft Lithography.* Science, 2002. **298**: p. 580-584.

92. Ros, A., *Microfluidics in Cell Analysis.* Analytical and Bioanlytical Chemistry, 2008. **390**(3): p. 1618-2642.

93. Kim, M.S., W. Lee, Y.C. Kim, and J.K. Park, *Microvalve-Assisted Patterning Platform for Measuring Cellular Dynamics Based on 3D Cell Culture.* Biotechnology and Bioengineering, 2008. **101**(5): p. 1005-1013.

94. Kim, S.H., J.H. Choi, S.K. Lee, S.M. Yang, Y.H. Lee, C. Seassal, P. Regrency, and P. Viktorovitch, *Optofluidic integration of a photonic crystal nanolaser.* Optics Express, 2008. **16**(9): p. 6515-6527.

95. Monat, C., P. Domachuk, and B.J. Eggleton, *Integrated optofluidics: A new river of light.* Nat Photon, 2007. **1**(2): p. 106-114.

96. Erickson, D., S. Mandal, A.H.J. Yang, and B. Cordovez, *Nanobiosensors: optofluidic, eletrical and mechanical approaches to biomolecular detection at the nanoscale.* Microfluidics and Nanofluidics, 2007. **4**(1-2): p. 1613.

97. Mandal, S. and D. Erickson, *Nanoscale optofluidic sensor arrays.* Optics Express, 2008. **16**(3): p. 1623-1631.

Chapter 2

Actuate-to-Open Valves

2.1. Introduction

Microfluidic devices that utilize actuate-to-close valves (AtC) have been implemented previously for a variety of applications including synthesis, separation, cell analysis and mixing [1-7]. These devices are comprised of microchannels that are between 150 and 500 μm wide and between 5 and 50 μm high. These devices use pico- to microliter volumes, and typically are operated in a continuous flow semibatch mode. For very small batch processes at sub-nanoliter volumes, a high reaction density is desirable. One method to achieve these high densities is to explore multilayer soft lithography [8]. Unfortunately, when these high density processes must be transported for analysis or screening, the AtC valves developed in this work must be continually attached and activated. As AtC valves are passively open, they require continuous connection to an ancillary pressure source at all times. Leaking issues can crop up using AtC valves in high-density systems, as pressurized compartments can deform, causing leaking of their contents into adjacent compartments, which makes the intricate coordination of mixing of reactant plugs very difficult. For microfluidic devices that require densities on the order of 1 reaction/mm^2, a different approach is needed to enable routing and mixing of fluid plugs.

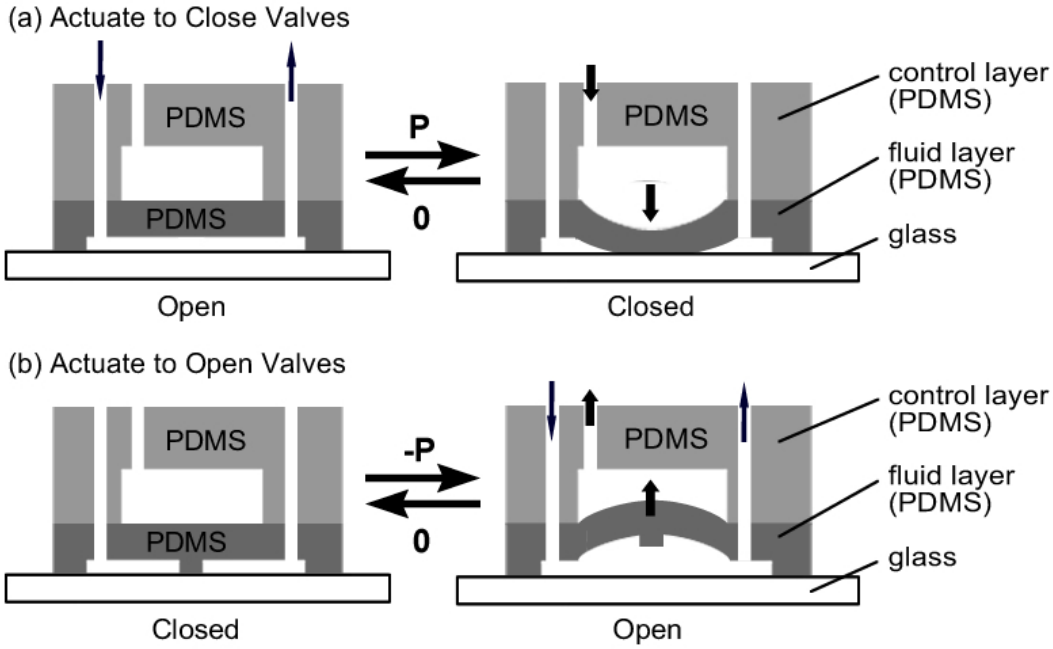

Figure 2.1. Schematic of an (a) Actuate-to-Close (AtC) and (b) Actuate-to-Open valve comprised of a pneumatic control layer and a fluid layer made from polydimethylsiloxane (PDMS). Both devices function as valve elements within multilayer microfluidic devices capable of fluid handling in volumes as low as picoliters in size.

Mathies *et al.* have explored an alternate valve design using passively closed valves using a flat-commercially available ductile membrane in between microchannels etched in glass [2, 9-12]. These valves also have the capability of switching out the PDMS membrane for a Teflon membrane for harsh systems or environments [13-15]. While these passively closed valves developed by Mathies *et al.* overcome some of the issues associated with the use of AtC valves, their specific design and the glass-based fabrication approach prevents the creation of microfluidic devices with a high density of functional components, such as arrays of compartments that can be isolated.

In response to these inadequacies, we developed actuate-to-open (AtO) valves that seal passively closed at rest (Figure 2.1). These valves are developed using the

multilayer soft lithography (MSL). When mixing or metering operations are finished, devices using these valves can be disconnected from pneumatic control lines and transported without interrupting any ongoing experiment within the chip. Because MSL is employed in fabrication, these AtO valves can be integrated in much higher densities ($1/mm^2$) than the Mathies valves ($1/cm^2$) [2].

The AtO valves remain passively closed at rest. Upon the application of vacuum, the valves lift these PDMS walls up to open passageways within the device. This vacuum also permeates into the fluid layer, due to the gas permeability of the fluid layer in the device. The vacuum creates a pump for the fluid in the device as well as an activation of valves to allow the pumping of liquid into the fluid channels. The overlap of the valves also leads to a tighter fit within the design. Because a separate area for valves and a separate area for liquid storage as in AtC systems is no longer needed, these AtO valves can achieve higher reaction densities.

These new valves open up new and exciting opportunities for on-chip combinatorial screening. Since the valves are closed in rest, these microfluidic chips can be decoupled from pneumatic pressure lines and transported mid-experiment without having to fear unwanted mixing of reactants or leakage from the device. Chapters 3 and 4 discuss the implementation of a 4 x 4 combinatorial screening device that employs the AtO valves, which can be decoupled from pressure sources for protein binding and virus identification, respectively. Other applications could benefit from this AtO valve, but deeper understanding of the factors that determine valve operation is required to guide their implementation into future chips [1, 16, 17]. This chapter looks at

variables that influence the operational parameters of the AtO valves, including microchannel width, membrane thickness, and microchannel geometry, to yield a set of design rules to guide the development of AtO-valve based microfluidic devices.

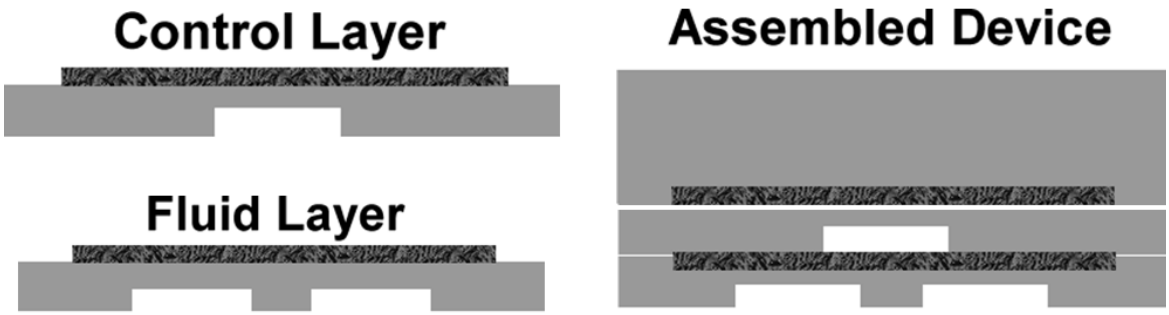

Figure 2.2. A schematic of electrostatic valve assembly. Both layers are prepared using PDMS on a silicon/photoresist substrate as per standard multilayer soft lithography fabrication. Nanotubes are stamped using a PDMS stamp to cover valves. PDMS layers are then cut out, aligned and permanently baked together to create a permanent seal between the layers. Electrodes are connected to the nanotube-based electrodes. Applying a potential difference between the two parallel electrodes will create the electrical force needed to open the valve. Typical PDMS layer and nanotube electrode thickness is 35 µm and 5 µm, respectively.

2.2. Results and Discussion

2.2.1 Design and Fabrication

Actuate-to-open valves are passively closed and are typically quite robust in operation, relying on a few physical principles that can influence the required pressure difference to open the valves. The valves are comprised of two layers of PDMS, which are permanently sealed together using the partial curing technique discussed in other work [1]. The valves are actuated pneumatically using a vacuum line connected to a scaffold, with tubes connected for the pressure inlets into the device.

In addition to pneumatic AtO valves, we also explored similar valve geometries that can be actuated electrostatically (Figure 2.2). Electrostatic actuation has the advantage

of not requiring an external pressure source, requiring smaller ancillary systems that vary the voltage. Electrostatic valves have been explored in the literature at centimeter to decimeter scale, but few have achieved dimensions of the AtO valves studied here at the micrometer to millimeter scale [18-20]. Valve operation could be performed at 170V for a 35 μm high microchannel, the first such observation for these AtO valves. This is much higher than desired for microchemical systems and further work needs to be performed to lower the required actuation voltage. Because these valves rely on capacitative forces between oppositely charged layers of nanotubes, reducing the distance in between the electrodes is important for reducing the voltage required to actuate. However, as the control valve is placed between the two electrodes, if the space between these electrodes is too small, the valve will collapse and will not function. For future work, these opposing variables will need to be finely balanced in order to reduce the required voltage for a fully operable valve.

Another known issue with electrostatic valve operation lies in the usage of nanotubes as electrodes. First attempts at valve design included stamped nanotubes onto a dry surface, which was encapsulated within fully cured layers of PDMS (Figure 2.3a,b). The valve, filled with these dry nanotubes, became dusty and would often delaminate. In order to correct for this delamination issue, an additional step was added for the fabrication process. Liquid PDMS was spun on top of the nanotubes, leaving the nanotube layer intact while encapsulating it in a thin layer of PDMS. By encapsulating the nanotube layer under a solid layer of PDMS that could be cured, individual nanotubes were not free to cluster and flocculate, leaving a more homogenous and

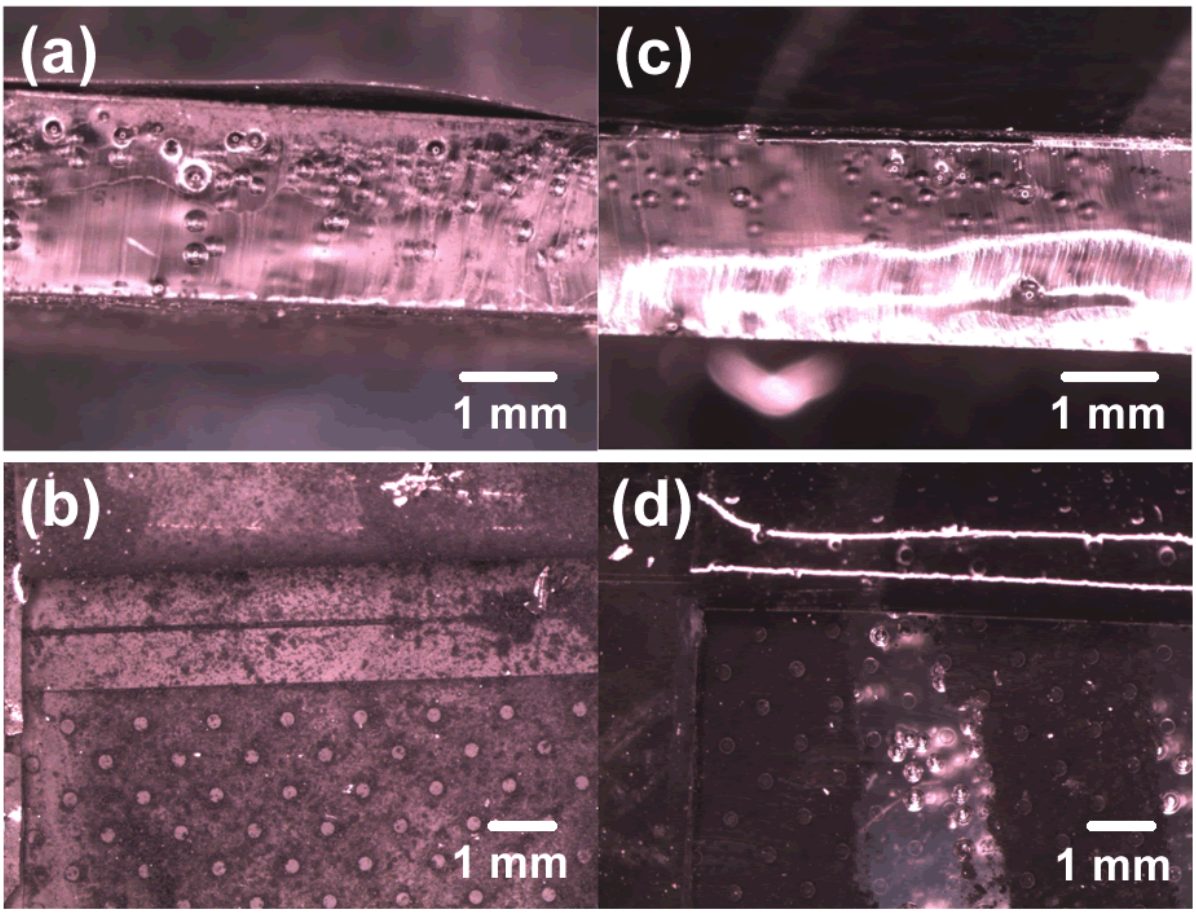

Figure 2.3. **(a)** A side view crosscut of dry encapsulated nanotube-based AtO valve. **(b)** A top view of a incision within a dry encapsulated nanotube-based AtO valve. **(c)** A side view crosscut of a wet encapsulated nanotube-based AtO valve. **(d)** A top view of an incision within a wet encapsulated nanotube-based AtO valve. Wet encapsulation is superior to dry encapsulation, because the nanotubes do not flocculate nor cause delamination, as seen in left photographs.

conductive electrode capable of holding charge (Figure 2.3c,d).

While the electrostatic valves were interesting for pressure-free device operation, they were not advanced far enough to be suitable in very large scale integrated microfluidic devices. For the purpose of screening applications, pressure-based AtO valves were optimized in this study. In order to develop arrays of valves, deeper understanding is required. Valve operation needs to be quantified as a function of design parameters. For this purpose, a number of parameters were examined to

discern their effect on the pressure required to open the valves.

Fluid microchannel width, valve asymmetry and membrane thickness affect how the valves actuate, and how the valves return to rest. Small changes in these variables were instituted in a microfluidic device using an actuate-to-open valve. The pressure required to operate the valves was then recorded and averaged on three runs for each experiment to determine their response and how important these variables are to operation.

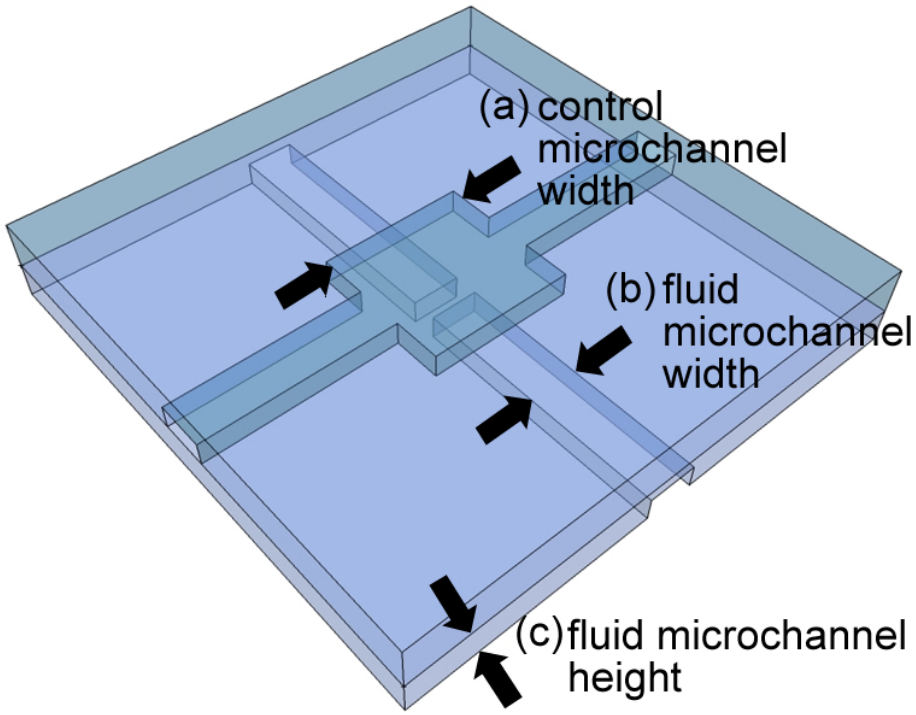

Figure 2.4. A schematic of the actuate-to-open (AtO) valve. For the purposes of these studies, the control microchannel width is denoted by (b), the fluid microchannel height is denoted by (b), and the fluid microchannel height is denoted by (c).
[© by Michael Thorson. Used with Permission.]

2.2.2. Operation

Devices are prepared using multilayer soft lithography (MSL) [1], discussed in detail in section 2.4. The final device is comprised of two layers of PDMS: a control layer and a fluid layer. These layers are permanently sealed together using partial curing, and reversibly sealed to a bottom substrate, such as glass. When the valve is at rest, the PDMS forms a seal based on van der Waals forces. When the valve is allowed to relax back to atmospheric pressure, the thin PDMS layer demonstrates a low resistance to deformation and requires very little pressure to remain open. Much of the energy spent in operating the valve is in the opening phase of the process overcoming van der Waals forces. This hysteresis in operation is shown in Figure 2.4.

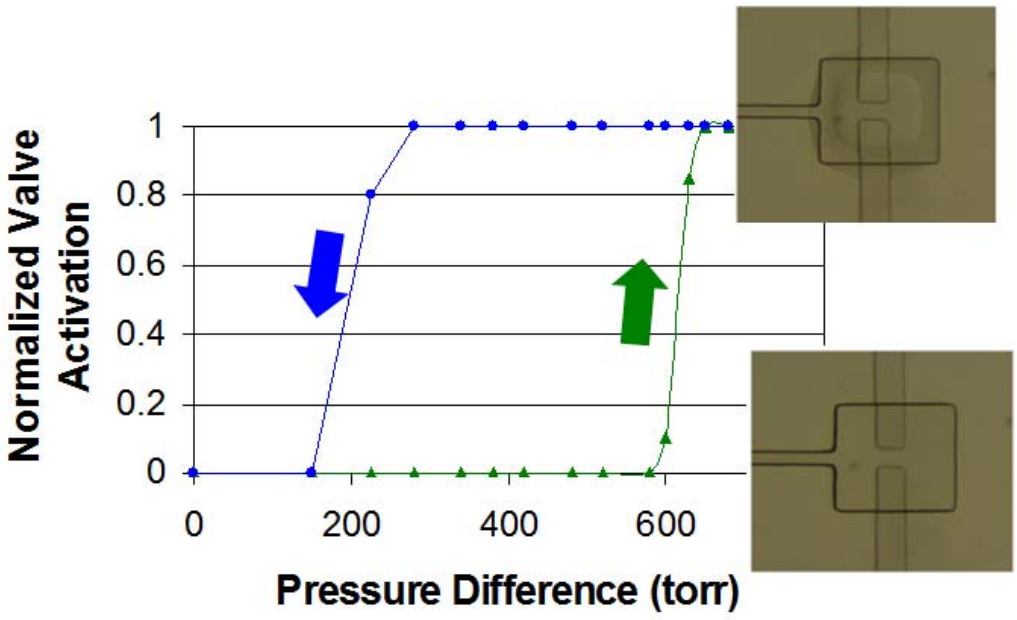

Figure 2.5. A graph of the required pressure to open actuate-to-open valves. Pressures can range from -200 to -650 torr for valve opening, and collapse at rest when little to no pressure is applied, depending on fluid layer thickness. The normalized valve actuation is defined as the amount of the PDMS inside the valve being lifted off the glass. 1=100% of the PDMS is lifted off the glass, where 0=no PDMS is lifted off of the glass.

This hysteresis is influenced by a number of factors, including fluid layer thickness, fluid microchannel width, and the geometry of the microfluidic channels, particularly the shape / placement of the PDMS obstruction in the microchannels that forms the valve (See Section 2.2.3). For example, in a fluid layer 40 µm in height, a 75µm x 25µm microchannel actuates with a 250 micron-wide valve seated over it at an actuation pressure difference of 600 torr. In order to operate the valves, this actuation pressure must overcome the van der Waals forces between PDMS and the substrate beneath it, which is typically glass.

The bulk of the valve actuation energy is due to opening the valve, essentially ripping the valve seat off of the glass surface. The valves close within milliseconds when vacuum is turned off. PDMS has a high Young's modulus; it stretches readily on the application of very little pressure. This hysteresis of the PDMS ripping off the glass can be tuned with the parameters of the device that highly affect the required pressure for opening and closing. Here, we will discuss how valve size, asymmetry and membrane thickness affect the results of the pressure required to open the valves.

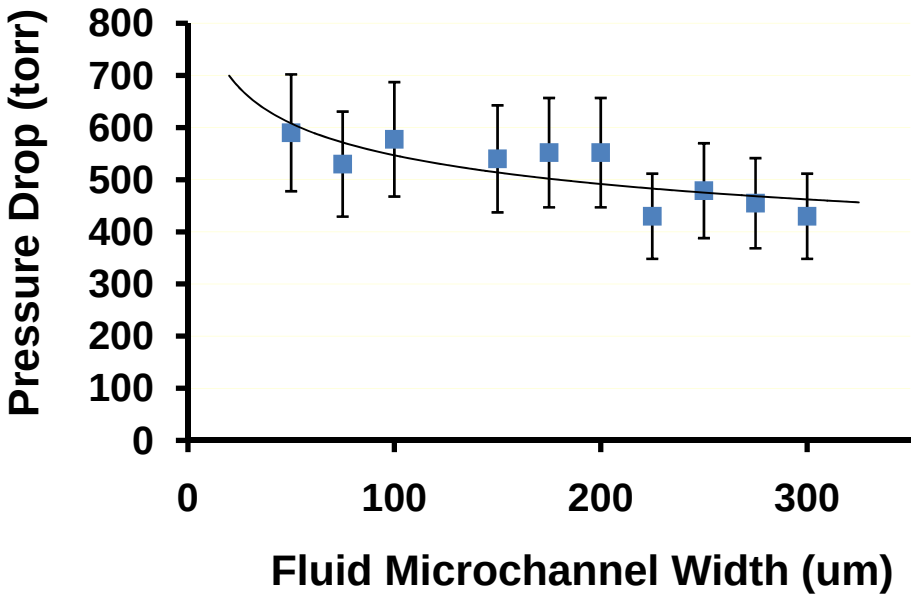

Figure 2.6. A graph of the valve response in terms of the pressure drop required to open the valve as a function of the fluid microchannel width. Variations in microchannel width underneath a constant valve width of 250 µm lead to changes in area underneath the valve. As the microchannel width decreases, the area contacted increases, and the pressure required to open the valve increases as well. The R-squared value for the above correlation is 0.76.

2.2.3. Design Rules

In order to elucidate the behavior of the valves, a series of experiments were performed to determine what effect valve compartment size, valve geometry and fluid membrane thickness has on the required pressure drop to open the valves. Since most of the pressure is converted into energy devoted to opening the valves, the pressure drop across the fluid membrane required to open the valves is the reported value for these studies. For all valves in these studies, the valves relaxed to rest only when the valves were exposed to atmospheric pressure. In all cases, the devices were prepared using MSL and all valves were opened fully at maximum vacuum pressure (650 torr), and allowed to collapse at rest for five minutes. The pressure difference was

incrementally increased by adjusting valves connected to the vacuum manifold, and the pressure drop that was large enough to open the valves was recorded.

2.2.3.1. Effect of Valve Size

Quake and others have determined design rules for monolithic AtC valves using experimental and computational methods [2, 21]. Variations in the widths of the microchannels in the control and fluid layers can dramatically change the amount of pressure required to operate these AtC valves. An analogous study must be performed in order to elucidate design rules of the AtO valving structures.

Variations in the control channel and the fluid channel cause differences in the amount of applied pressure required to open AtO valves. Other factors, including fluid membrane thickness and valve shape contribute to the required activating pressure as well. As a channel becomes larger and larger in size, valves require less applied pressure to open. A pressure drop of 200 torr was observed for most valves between 125 and 300 μm in width. As the channels become smaller, in the range of 50 to 125 μm, the valves require more of a pressure drop to open. The fluid microchannels are filled with atmospheric pressure, and as their widths become small, there is less area for this atmospheric pressure to push up against the vacuum. Additionally, when comparing two control channels of equal size over two different fluid microchannels, the smaller fluid channel not only has less area for atmospheric pressure to push up against, it also has a larger area of PDMS to pull up off of the glass surface.

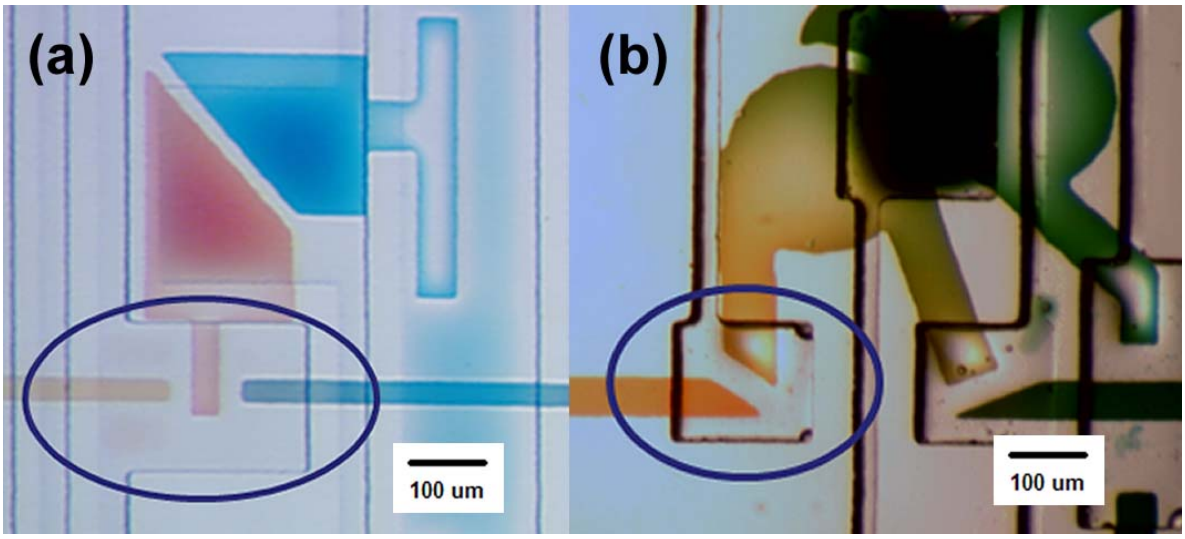

Figure 2.7. Optical micrographs of two half-wells with AtO valves controlling flow. (a) The valve within the blue oval is in a symmetrical arrangement, and it required pressures of -13 psi to activate. (b) The valve within the blue oval has an asymmetrical element, and required only -8 psi to open. This difference is due in part to weak points introduced within the design of the fluid lines, making the valves require less pressure to open.

2.2.3.2. Effect of Valve Asymmetry

During the evolution of the combinatorial screening chip developed in Chapter 3, it was observed that different geometries in the shape of the fluid microchannels required vastly differing valve actuation pressures. Figure 2.7 shows two sets of microfluidic valves with the same contact area but different relative arrangement and shape of the fluid channels. The more asymmetric design could be opened with a lower vacuum. This effect is caused by weak points introduced within the microfluidic device, as observed in other studies [22, 23]. To quantify this effect, we introduced elements of asymmetry within the fluidic lines and studied the effect that variations in geometry might have on the pressure required to open the valves.

First, a series of microchannels terminating in acute and obtuse angles was studied. Microchannels were fabricated as discussed previously, except they were designed to

be millimeters in length, to provide for generous overlap of the fluid channel with the valve actuation compartment. The original overlap of the valves was utilized as a design feature for ease of assembly, however such generous overlap proved to be a source of error in data collection. In this experiment, terminal geometry did not reveal a statistically significant variation in pressure response. Further details regarding the experimental design revealed the extent to which the control valves overlapped the fluid microchannels. In particular, a major source of error was created by creating such a high amount of overlap. An observed correlation between high overlap and lower pressures led to the understanding that if the exposed perimeter underneath a valve was increased, the terminal geometry had little effect (Figure 2.8). Valves would initially open from the side, rather than the terminal point, nullifying any effect those terminations might have as a starting point for valve opening.

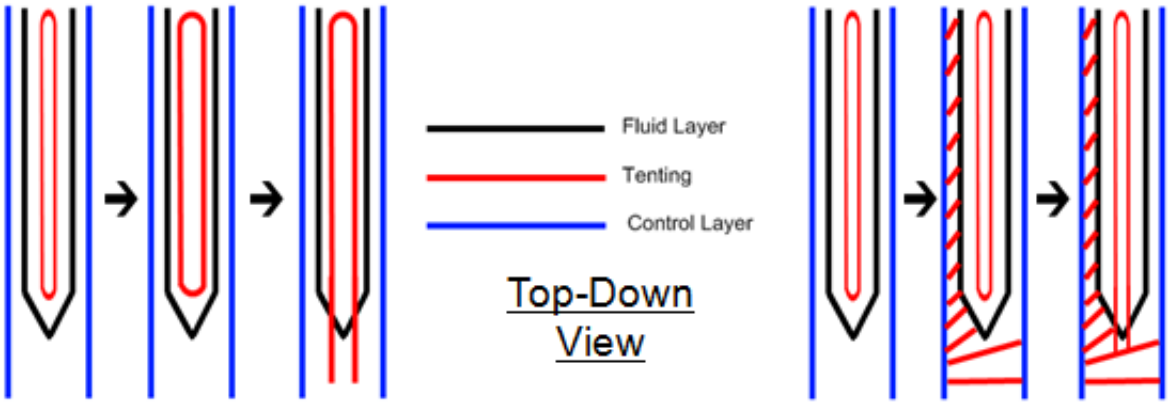

Figure 2.8. A schematic of how a series of valves open over time. (left) If the valve (blue line) begins to lift upward (red line) closer to the perimeter of the microchannel (black line) and opens at the bottom first, the terminal geometry will influence at what pressure the valve will open. (right) However, if there is significant overlap of 2-3 cm, the valves will lift open at the side portion of the perimeter, thus nullifying any effect that terminal geometry may have on the valve opening.

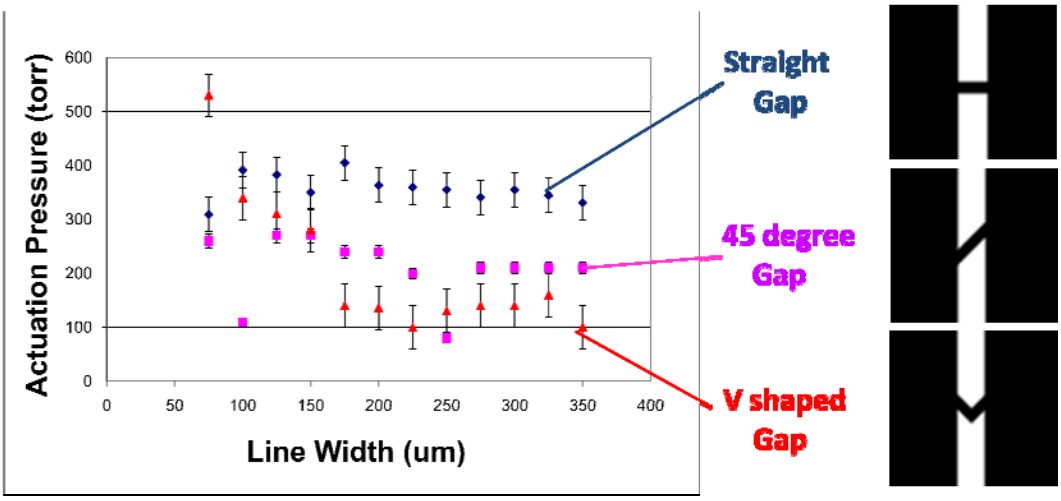

Figure 2.9. A graph of the required pressure difference to activate valves with a straight gap (2 lines of symmetry), a slant shape (1 rotational symmetry) and a v-shaped gap (1 line of symmetry with focus point). The v-shaped gap is the easiest valve to open and requires the least pressure. This is to be expected, since the atmospheric pressure within the fluid channel can concentrate on lifting the exposed corner of the device.

To sidestep the issues that arise from long perimeters of fluid channel, a new experiment was designed that limited the area of the control channel to 350 µm x 350 µm. Three shapes, a straight line, a diagonal line and a v-shaped gap, were used to determine the effect of 2 symmetry lines, 1 symmetry rotation and 1 symmetry line on the required activation pressure, all focused underneath these control channels. Adhesive studies have shown that by focusing forces onto a point (v-shaped gap), a noticeable drop in required lifting force is observed [24-26].

As observed in Figure 2.9, the introduction of asymmetry elements reduced the pressure required to operate the valves, in some cases by as much as 50 torr. These asymmetry elements serve as focal points for the pressure forces within the fluidic microchannel, which reduce the overall pressure required to open the valves. When the straight valve is employed, forces can be balanced on both sides of the valve equally

amongst all four sides of the rectangular shape beneath the control valve. By creating a slant 45 degree angle underneath, when the fluid microchannel begins to tent under vacuum, the nearby obtuse angle of the microchannel perimeter is closest to the center of lift under the valve. This portion of the valve is lifted first, on either side of the PDMS gap, and these valves require less pressure to operate due to the focusing of forces on these obtuse angles. The final V-shaped valve required the least amount of pressure, because instead of an obtuse angle being exposed to the center of lift first, a convex corner was exposed first. This focused the lift not just on a particular side first, but on an exposed corner, which allowed for easier lift on one side of the microchannel.

One interesting result of this experiment is the amount of error observed for all valve shapes, except for the diagonal 45 degree valves. Each set of error here is generated by three separate devices, so it is possible that this type of valve is the least resistant to misaligning in the device. Both the straight valves and the v-shaped valves, if misaligned by 10-50 micrometers, would cause drastic variations in the pressure required to operate the valve. The diagonal valves did not exhibit this change, because variations of 10-50 micrometers could be compensated by the geometry of the microchannels. Because of this reliability, the diagonal 45 degree valves were utilized whenever possible in the combinatorial screening chips discussed in Chapters 3 and 4.

2.2.3.3. Effect of Membrane Thickness

The absolute thickness of the fluid layer also contributes to the operational parameters. PDMS is gas permeable, so when the fluid layer becomes too thin, vacuum is not maintained for very long within the control layer. Instead of atmospheric

or water vapor pushing up on the bottom of the device, air diffuses from the microchannel through the membrane into the control layer and the valve does not actuate.

We studied the effect of membrane thickness on valve actuation pressures (Table 2.1). While no statistically significant variation was observed for thicknesses between 27-40 μm, the thickness of 44 μm was observed to have a higher pressure requirement. At thicknesses lower than 27 μm, the valves would not operate up to a pressure difference of 650 torr, which was the full gauge pressure of the vacuum supply used for this experiment. Above 44 μm, the valves would also not operate at this full vacuum pressure. It is possible that two effects are simultaneously competing to reduce the actual pressure difference across the membrane. The gas permeability of the PDMS fluid layer is a function of thickness, so it is possible that a large pressure drop cannot be achieved, since gas would leak from the atmospheric pressure in the fluid layer into the control channel. The localized Young's modulus is also a function of fluid layer thickness, so it is possible that at 44 μm and above a much higher pressure is required for valve operation. As a design rule, it is important to fabricate a device that does not succumb to either of these extremes, preferably between 27 and 40 μm in height.

Membrane Thickness (μm)	Required Pressure Drop (torr)
10	-
20	-
27	340 ± 40
34	330 ± 40
40	380 ± 60
44	500 ± 50
49	-
52	-
59	-

Table 2.1. Fluid layer thicknesses varying from 10 to 59 μm were tested using 200 μm square valves over a 100 μm wide fluid microchannel. Below 27 μm, the valves did not actuate due to the membrane layer being so thin that air passed through the layer rather than open. Above 44 μm, the layer was too thick to bend properly within the small control layer size. The local minimum and best thickness for these valves is 34 μm.

2.3. Conclusions

The power of microfluidic devices come from the ability to scale out. Vast arrays of valve-based networks must be created in order to perform many analyses in parallel. However, further scaling out of the AtO valves discussed in this chapter is not as trivial as just expanding the control layer networks for valve actuation. PDMS, the polymer typically used for these microfluidic devices fabricated via MSL, is very permeable to gas, which places limitations on the design of vast microfluidic networks. Sustaining sufficient pressure drops for valve actuation across the whole chip would be difficult. To that end, it is important to understand exactly how much of a pressure difference is required for the valves to operate reliably. Here the pressure actuation requirements for valve operation as a function of fluid microchannel width, fluid layer thickness and microchannel geometry were studied. Further study is needed to precisely quantify the pressure losses down a series of valves still will be needed.

In the studies reported here, variations in fluid microchannel width and microchannel geometry resulting in significant changes in the pressures required to actuate the valves (dP on the order of 200 torr). For the most part, these results were expected. As pressure is defined as force acting on a certain area, this means that a larger valve actuation compartment translates to a stronger force exerted on the fluid layer underneath.

In early instances of valve failure, it was typically due to the design of the shape of the valve. When valves could not be opened, the root cause was either a fabrication issue (e.g. misalignment) or a geometry issue (e.g. insufficient valve compartment area, too thick or too thin fluid layer). PDMS seals tightly with many surfaces, including glass, due to strong van der Waals forces. To overcome these van der Waals forces to open the valve requires the introduction of weak points within the valve design, such that lower actuation pressures suffice. In terms of design, the valve shape that would require the highest actuation force would be perfectly circular in nature. As the pressure drop increases across the fluid layer membrane, the force caused by this difference in pressure can be mitigated and balanced all throughout the circular microchannel. This leads to a higher pressure difference required to lift the valve. However, if an asymmetry element is introduced into the valve design , a weak point is created where the valve seat can start to delaminate from the glass surface. Once a valve begins to open, typically the rest of the surface is easily ripped upward, as observed in other studies [27-29].

Given the nature of the elasticity of PDMS, it was expected that alterations in fluid layer thickness would have had a substantial effect on valve actuation pressure, but this was not observed to be the case. Variations between 27 and 44 μm did not create large differences in pressure requirements for the valve. And when this range was expanded, valve failure was experienced in cases where the fluid layer was too thin or too thick. When the PDMS was too thin (<27 μm), air permeated easily through the control layer leading to insufficient pressure differences across the membrane. When the layer was too thick (>44 μm), the PDMS layer was not easily deformable underneath the control channel, again causing the valve to resist from being actuated. In summary, as a design rule, we determined a narrow range of membrane thicknesses that yield functional valves.

After these valves were studied as to their use and the design rules that affect their operation, they were subsequently employed in a combinatorial design studying protein-antibody assays (Chapter 3) and in a multiplex DNA sensing chip for virus identification (Chapter 4).

2.4. Materials and Methods

2.4.1. Device Fabrication

For the experiments in this section, the microfluidic device is built using multilayer soft lithography [8]. The control layer and fluid layer designs are crafted using Freehand MX, with careful attention to the dimensions of the valves using the in-product ruler. The designs are laser printed by the University of Illinois Print Shop (5080 dpi) onto a

negative transparency mask. The areas of the microchannels are clear, which allows UV light to pass through and harden a thin layer of SU-8 negative photoresist, spun onto clean silicon wafers at 2000 RPMs. After exposure of UV light at 10.8 mW/cm^2 for 30 seconds, they are developed for one minute in PGMEA (propylene glycol monomethyl ether acetate). The solvent is rinsed off using isopropyl alcohol and then dried under nitrogen. The resulting silicon wafers (masters) are then surface treated for four hours using a silanizing agent to render them hydrophobic.

Next PDMS (polydimethylsiloxane) is prepared in 15:1 and 5:1 ratios of monomer:crosslinker in total amounts of 10g and 50g each. These materials are mixed vigorously and degassed using vacuum coupled to a dessicator. The 15:1 PDMS is poured onto the master for the fluid layer and spun at 2000 RPMs in a spin coater, while the 5:1 PDMS is poured onto the master for the control layer to a thickness of ~2 mm. Both layers are cured at 65°C for 35 minutes, and then the control layer is cut out and holes are punched to provide inlets for the valves in the control layer. The control layer is then aligned to the fluid layer, and the assembled device is placed in the 65°C oven for 1 hour to complete the irreversible seal between the layers.

The device is then cut out from the remaining fluid layer and placed onto a substrate, typically a glass slide, cleaned with acetone and isopropanol prior to use. For the measurements above, all valves are actuated fully and lifted off of the glass surface, allowed to relax back to rest and then measurements are begun immediately to avoid polymer chains in the PDMS reorganizing to create a very strong seal with the glass over time.

2.4.2. Pressure Readings

For all studies performed in this chapter, the microfluidic devices were prepared according to the above protocol, and allowed one day to fully cure at room temperature. The device was then pulled off of the glass surface and placed onto a cleaned glass slide. A vacuum source was hooked up to a scaffold through a ball valve and a pressure gauge, which was then hooked up to the microfluidic device using polypropylene tubing and metal tubes as shown in schematic (Figure 2.10).

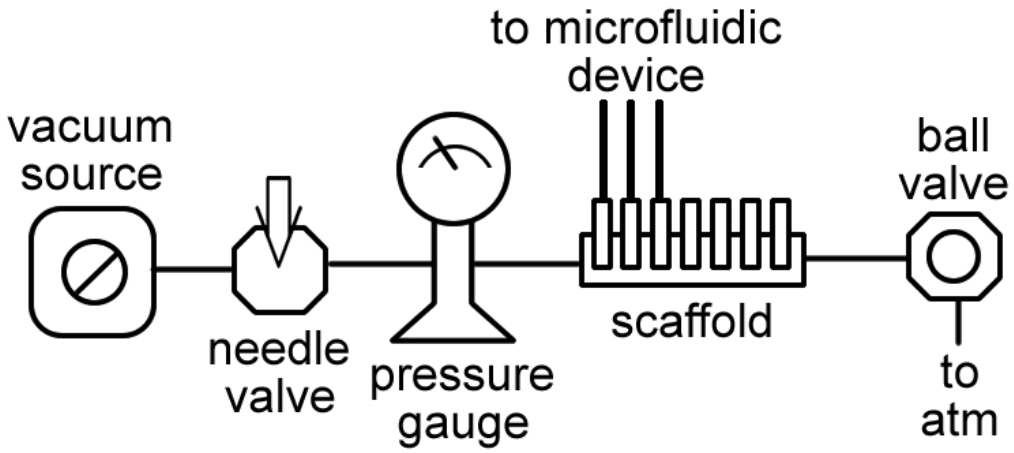

Figure 2.10. A schematic of the connections and valves for the design rule experiments. A vacuum source (maximum pressure 650 torr) was fed into a needle valve through Nalgene PVC tubing, which entered a three-way teflon valve connected to a pressure gauge. The line continued through Nalgene PVC tubing to a scaffold, where the connection fed through seven three-way valves that could be independently operated to control valves in a microfluidic device. At the end of the scaffold, a ball valve was used as an atmospheric inlet to collapse valves to rest as well as balance the pressure in a steady state fashion.

To begin the experiment, the valves were connected to full vacuum (ball valve closed, needle valve fully opened, scaffold 3-way valves open). This forced all valves to be open, as well as serve as a crosscheck to make sure the device was fully operable. The valves were then allowed to collapse back to rest for 5 minutes in the fully closed position (needle valve fully closed, ball valve open, scaffold 3-way valves fully open).

The 3-way valves of the scaffold were then closed, and the ball and needle valves were adjusted to achieve a steady pressure reading on the pressure gauge. The 3-way valves leading to the microfluidic device would then be opened and the valve operation would be recorded. The 3-way valve was then turned to open to atmospheric pressure to allow the valves to close back to rest state. If the valve opened within 3 seconds of exposure to vacuum, this pressure was considered the operating pressure and this value was subtracted from the atmospheric pressure for that day. This resulted as the pressure difference recorded in the graphs and table in this chapter.

2.5. References

1. Thorsen, T., S.J. Maerkl, and S.R. Quake, *Monolithic Microfabricated Valves and Pumps by Multilayer Soft Lithography.* Science, 2002. **298**: p. 580-584.
2. Grover, W.H., A.M. Skelley, C. Liu, E.T. Lagally, and R.A. Mathies, *Monolithic membrane valves and diaphragm pumps for practical large-scale integration into glass microfluidic devices.* Sensors and Actuators B, 2003. **89**(3): p. 315-323.
3. Urbanski, J.P., W. Thies, C. Rhodes, S. Samarasinghe, and T. Thorson, *Digital microfluidics using soft lithography.* Lab on a Chip, 2006. **6**: p. 96-104.
4. Wheeler, A.R., W.R. Throndset, R.J. Whelan, A.M. Leach, R.N. Zare, Y.H. Liao, K. Farrell, I.D. Manger, and A. Daridon, *Microfluidic Device for Single-Cell Analysis.* Analytical Chemistry, 2003. **75**(14): p. 3581-3586.
5. Zhao, X.-M., Y. Xia, and G.M. Whitesides, *Soft lithographic methods for nano-fabrication.* Journal of Materials Chemistry, 1997. **7**(7): p. 1069-1074.
6. Galas, J.C., J. Torres, M. Belotti, Q. Kou, and Y. Chen, *Microfluidic tunable dye laser with integrated mixer and ring resonator.* Appl. Phys. Lett., 2005. **86**: p. 264101.
7. Chou, H.-P. and M.A. Unger, *A Microfabricated Rotary Pump.* Biomedical Microdevices, 2004. **3**(4): p. 323-330.
8. Unger, M.A., H.-P. Chou, T. Thorsen, A. Scherer, and S.R. Quake, *Monolithic Microfabricated Valves and Pumps by Multilayer Soft Lithography.* Science, 2000. **288**(5463): p. 113-116.

9. Lagally, E.T., P.C. Simpson, and R.A. Mathies, *Monolithic integrated microfluidic DNA amplification and capillary electrophoresis analysis system.* Sensors and Actuators B: Chemical, 2000. **63**(3): p. 138-146.

10. Lagally, E.T., C.A. Emrich, and R.A. Mathies, *Fully intergrated PCR-capillary electrophoresis microsystem for DNA analysis.* Lab on a Chip, 2001. **1**: p. 102-107.

11. Grover, W.H., A.M. Skelley, C.N. Liu, E.T. Lagally, and R.A. Mathies, *Monolithic membrane valves and diaphragm pumps for practical large-scale integration into glass microfluidic devices.* Sensors and Actuators B: Chemical, 2003. **89**(3): p. 315-323.

12. Grover, W.H., R.H.C. Ivester, E.C. Jensen, and R.A. Mathies, *Development of multiplexed control of latching pneumatic valves using microfluidic logical structures.* Lab on a Chip, 2006. **6**: p. 623-631.

13. Grover, W.H., M.G. von Muhlen, and S.R. Manalis, *Teflon films for chemically-inert microfluidic valves and pumps.* Lab on a Chip, 2008. **8**(6): p. 913-918.

14. Willis, P.A., F. Greer, M.C. Lee, J.A. Smith, V.E. White, F.J. Grunthaner, J.J. Sprague, and J.P. Rolland, *Monolithic photolithographically patterned Fluorocur PFPE membrane valves and pumps for in situ planetary exploration.* Lab on a Chip, 2008. **2008**(Advance Articles): p. DOI: 10.1039/b804265a.

15. Willis, P.A., B.D. Hunt, V.E. White, M.C. Lee, M. Ikeda, S. Bae, M.J. Pelletier, and F.J. Gunrthaner, *Monolithic Teflon membrane valves and pumps for harsh chemical and low-temperature use.* Lab on a Chip, 2007. **7**: p. 1469-1474.

16. Melin, J. and S.R. Quake, *Microfluidic Large-Scale Integration: The Evolution of Design Rules for Biological Automation.* Annual Review of Biophysics and Biomolecular Structure, 2007. **36**(1): p. 213-231.

17. Heckele, M. and W.K. Schomburg, *Review on micro molding of thermoplastic polymers.* Journal of Micromechanics and Microengineering, 2004. **14**(3): p. R1.

18. van der Wijngaart, W., H. Ask, P. Enoksson, and G. Stemme, *A high-stroke, high-pressure electrostatic actuator for valve applications.* Sensors and Actuators A: Physical, 2002. **100**(2-3): p. 264-271.

19. Goodwin-Johansson, S.H. and G.E. McGuire, *Microelectromechanical flexible membrane electrostatic valve device and related fabrication methods*, U. States, Editor. 2003, MCNC, Research Triangle Park: USA.

20. Bosch, D., B. Heimhofer, G. Mück, H. Seidel, U. Thumser, and W. Welser, *A silicon microvalve with combined electromagnetic/electrostatic actuation.* Sensors and Actuators A: Physical. **37-38**: p. 684-692.

21. Kartalov, E.P., A. Scherer, S.R. Quake, C.R. Taylor, and W.F. Anderson, *Experimentally validated quantitative linear model for the device physics of*

elastomeric microfluidic valves. Journal of Applied Physics, 2007. **101**: p. 064505.

22. Sofla, A., E. Seker, J.P. Landers, and M.R. Begley, *PDMS-GLASS Interface Adhesion Energy Determined Via Comprehensive Solutions for Thin Film Bulge/Blister Tests.* J. Appl. Mech., 2010. **77**(3): p. 031007.
23. Newby, B.-m.Z.C., Manoj K., *Effect of Interfacial Slippage on Viscoelastic Adhesion.* Langmuir, 1997. **13**: p. 1805-1809.
24. Verdier, C. and G. Ravilly, *Peeling of polydimethylsiloxane adhesives: The case of adhesive failure.* Journal of Polymer Science Part B: Polymer Physics, 2007. **45**(16): p. 2113-2122.
25. Vanitparinyakul, S., P. Pattamang, A. Chanhom, B. Tunhoo, T. Thiwawong, S. Porntheeraphat, and J. Nukeaw, *Study of PDMS compounds using the adhesion force determined by AFM force distance curve measurements.* Advanced Materials Research, 2010. **93**: p. 141-144.
26. Chaudhury, M.K. and M.J. Owen, *Adhesion Hysteresis and Friction.* Langmuir, 1993. **9**: p. 29-31.
27. Ahn, D. and K.R. Shull, *JKR Studies of Acrylic Elastomer Adhesion to Glassy Polymer Substrates.* Macromolecules, 1996. **29**(12): p. 4381-4390.
28. Hsia, J.K., Y. Huang, E. Mendard, J.-U. Park, W. Zhou, J. Rogers, and J.M. Fulton, *Collapse of stamps for soft lithography due to interfacial adhesion.* Appl. Phys. Lett., 2005. **86**: p. 154106.
29. Fujii, T., *PDMS-based microfluidic devices for biomedical applications.* Microelectronic Engineering, 2002. **61-62**: p. 907-914.

Chapter 3

Combinatorial Screening Chip Using Photonic Crystal Biosensors

3.1. Introduction

The first step in drug discovery is identifying a protein candidate that plays a key role in biological pathways that are believed to be involved in a disease. After such a key protein has been identified and its function in certain biological pathway is understood, screening for small molecules that could bind to the protein and thereby possibly inhibit its function can commence. New understanding has shown a variety of effects that the genetic code of protein has on function and interactivity [1-6]. Drug discovery involves a constant iterative cycle of libraries of small molecules that must be tested for their biological activity, which can be done computationally [7-9] and experimentally [10-14].

The main challenge in drug discovery studies lies in the truly vast parameter space [15-17]. Small changes in organic structure of a molecule can lead to vastly different biological activity, leading to thousands of possible compounds that must be screened for activity. Massive screening efforts of small molecules for their binding with target proteins are needed to identify potential leads for future pharmaceuticals. The screening of thousands of libraries requires a huge investment in time and money.

This chapter will discuss a new method of combinatorial screening at picoliter scales using microfluidic well plates for both the synthesis and screening of a protein against a series of bimolecular reactions all performed on chip in concert (Figure 3.1).

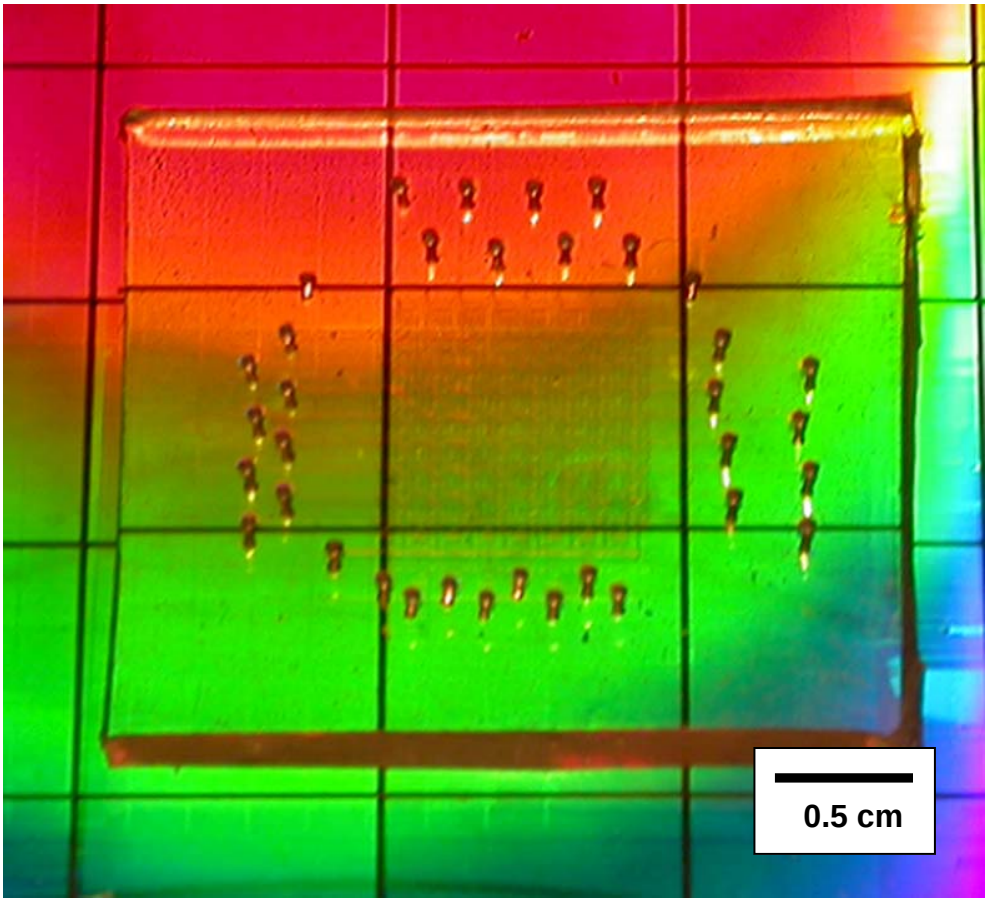

Figure 3.1 A photograph of an 8 x 8 microfluidic combinatorial screening chip placed on an photonic crystal biosensor surface. The microfluidic device here is fabricated using MSL, with AtO valves that rely on a reversible seal, which allows for the sensor surface to be exchanged as necessary.

3.2. Results and Discussion

3.2.1. Implementation of AtO Valves

A major benefit of the actuate-to-open valves discussed in Chapter 2 is its passively closed nature. Valves in everyday life as well as in most industrial applications are closed most of the time. So ideally a microfluidic device incorporates valves that are

closed in rest, such that no actuation is needed most of the time. Figure 3.2 demonstrates the filling procedure for operation of these valves. In this 8 x 8 microfluidic chip, one set of valves were opened, permitting flow in one direction of the chip (vertical). For chip operation, reagent droplets 3 µL in volume are deposited at the fluid channel inlets on the surface of the chip, where they can be subsequently channeled into the device by the application of vacuum to the set of AtO valves associated with that column or row. This method offers a way to introduce a particular reagent over a series of individual compartments within the chip, in each of which it will be combined with a different second reagent (see below), thus maximizing the experimental value of precious little reagent.

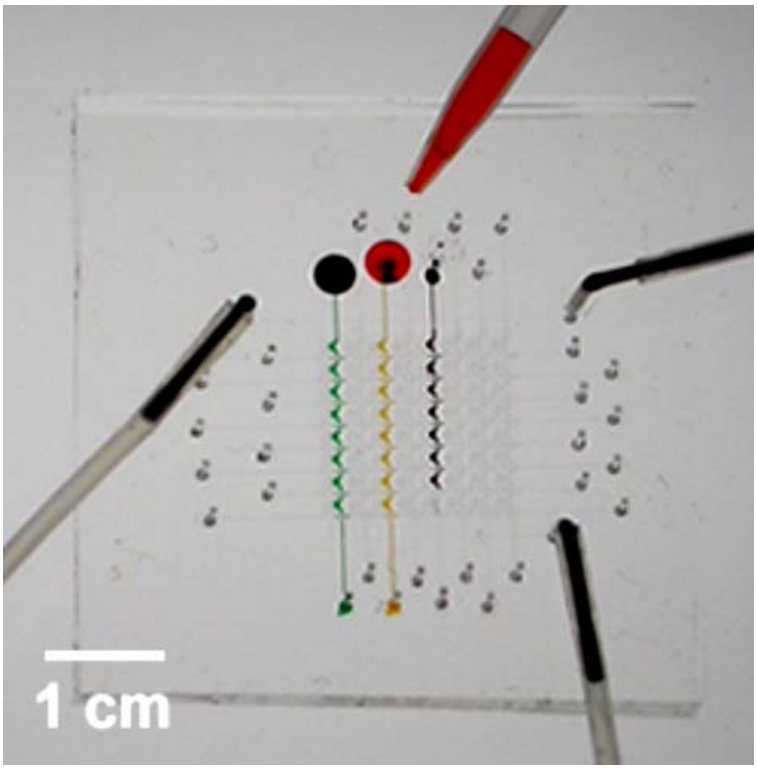

Figure 3.2. A photograph of an 8 x 8 microfluidic screening chip demonstrating the method used to fill columns of 200-pl compartments. Inlets for valves, shown by tubes here in the upper left, upper right and lower right, are activated by vacuum for filling. Reagents can be pipetted directly onto the inlet of each of the fluid channels (rows and columns), and then the fluid can be pulled into the chip by actuation of the AtO valves, or by applying a negative pressure at the opposite inlet.
[Reproduced by permission of The Royal Society of Chemistry (RSC), [18]]

The final design of the combinatorial microfluidic chip was scaled to a 4x4 array, yielding 16 combinations. The chip is configured such that a well density of 1 reaction/mm^2 was obtained The valves were arrayed in concert, so three separate valves (Figure 3.2) would have control over: horizontal filling of half-wells (small black valves), vertical filling of half-wells (rectangular orange valves) and mixing between the U-shaped half-wells (square red valves). For a given well composed of two U-shaped 200 picoliters half-wells, these valves can be operated to fill the right side half-well using horizontal valves, fill the left side half-well using the vertical valves, and open the mixing valve between the two half-wells. All thirty-two half wells can perform these actions in concert, mixing sixteen separate and different combinatorial reactions on a single microfluidic chip.

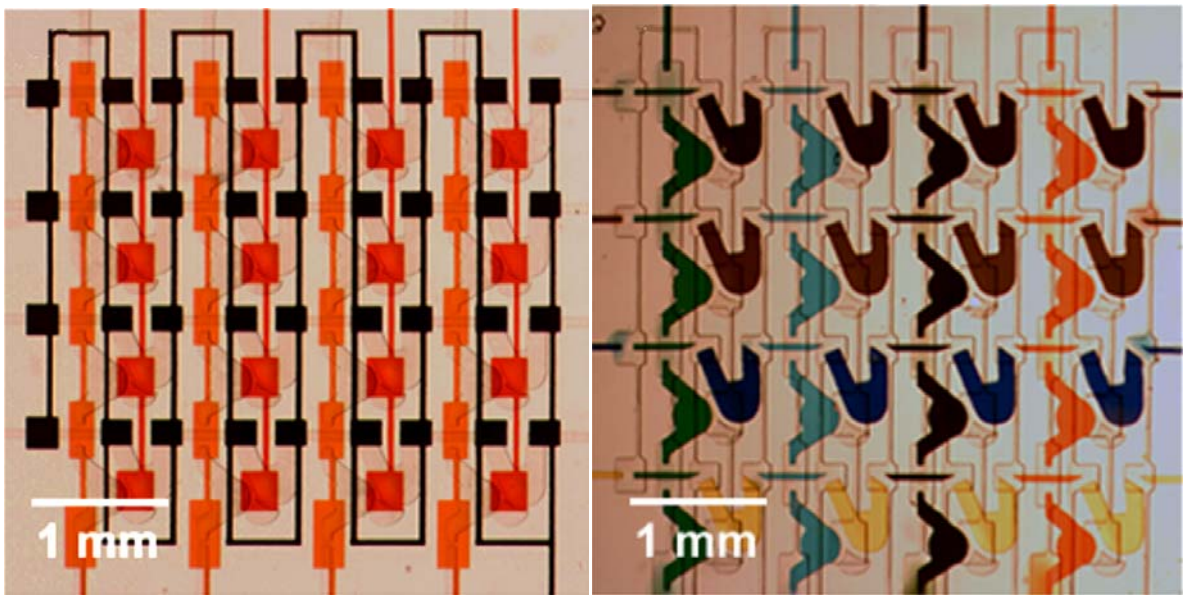

Figure 3.3. (left) An optical micrograph of the three valves of the control channel, filled with dye. (right) An optical micrograph of the fluid layer, with different dyes used to demonstrate the various rows and columns interconnectivity.
[Reproduced by permission of The Royal Society of Chemistry (RSC), [18]]

3.2.2. Integration with Photonic Crystal Biosensor

Analysis within the chip is performed using patterned photonic crystal biosensors, which have been used previously for kinetic studies of protein-substrate binding at the microscale [19]. These sensors, 250 μm in diameter, are centered within each U-shaped half compartment. Within each half-well, a biosensor can act as both a control and an experiment for a proof-of-principle binding experiment using a protein-antibody assay.

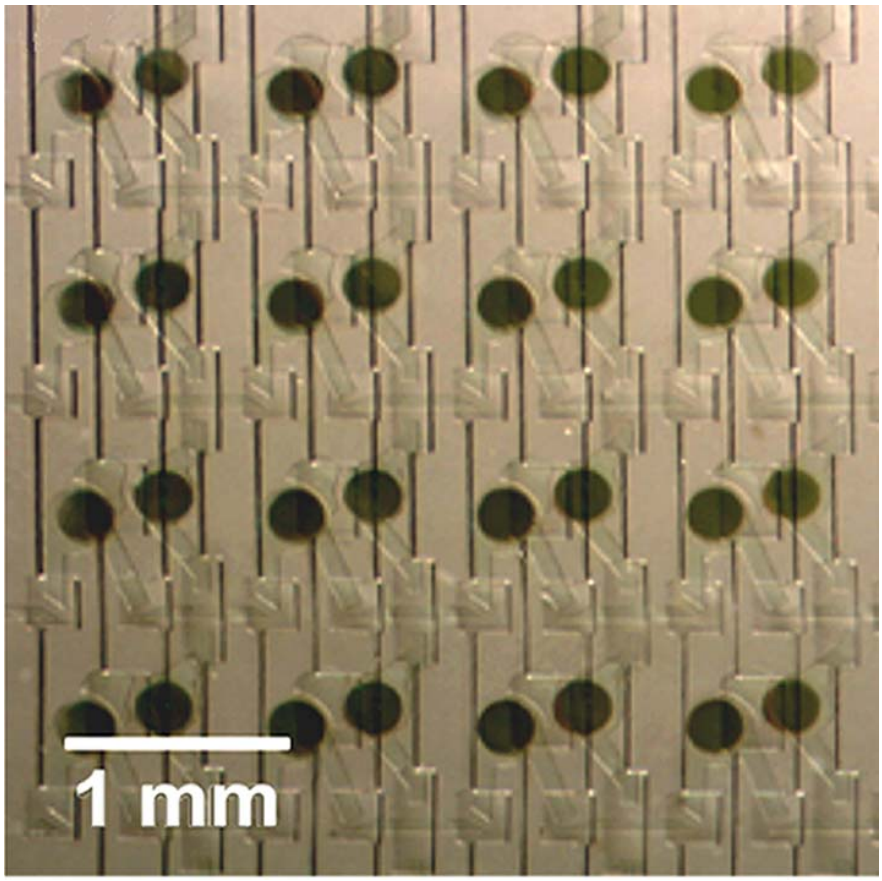

Figure 3.4. An optical micrograph of the combinatorial screening chip placed on a surface patterned circles of the photonic crystal biosensor. The circular biosensors, 250 um in diameter, are patterned to avoid leakage between half-wells of the chip.
[Reproduced by permission of The Royal Society of Chemistry (RSC), [18]]

After fabrication using MSL, the bottom layer of the device is reversibly sealed to the patterned photonic crystal sensor surface. Previous integration attempts of the

combinatorial screening chip with uniform photonic crystal biosensor surfaces encountered problems with respect to compartment to compartment leaking through the 500-nanometer grooves that comprise these biosensors surfaces. To avoid this leakage, the photonic crystal biosensor surface was patterned into 250 μm wide circles. To prepare the device for protein-based binding experiments, the entire device was built inside a clean room to reduce the amount of particulates that may enter the chip. After fabrication and sensor integration is complete, all wells of the microfluidic chip are filled with phosphate buffer solution and incubated for 24 hours.

3.2.3. On-Chip Protein/Antibody Binding Assay

As a proof-of-principle, a protein-antibody assay was employed within the combinatorial screening chip to validate the fidelity of the photonic crystal biosensor and microfluidic control within the chip. Protein A/G and protein A solutions were incubated in the right-hand half-wells of the 2nd and 4th rows, respectively. After incubation was complete, all rows were rinsed and loaded with phosphate buffer solution. In order to reduce nonspecific binding, both wells were coated with Sea Block agent, a salmon protein used to coat the exposed surfaces of the wells. When the incubation of Sea Block was finished, all wells were rinsed with phosphate buffer solution. Goat, chicken and human IgG antibodies were then introduced in the columns, thus entering the left hand wells, and a background scan was taken. Next, the mixing valves between the adjacent compartments were opened and diffusive mixing was allowed to occur for 30 minutes. During this time IgG antibodies can interact with the protein patterned surfaces in the right hand wells as well as with blank control surfaces in the left hand wells. At the conclusion of the 30 minute mixing time, the device was scanned again to

determine whether any binding occurred within each right hand half-well. Next, earlier recorded background was subtracted. As IgG antibodies bound to the surface, the change in the index of refraction of the material on the surface of the biosensor shifted in max wavelength value. Figure 3.5 shows the scan after background subtraction. This data is then converted into a histogram to quantify the extent of binding interaction between the various protein and antibody combinations (Figure 3.6). These results are expected as compared to prior work with these proteins and antibodies [20].

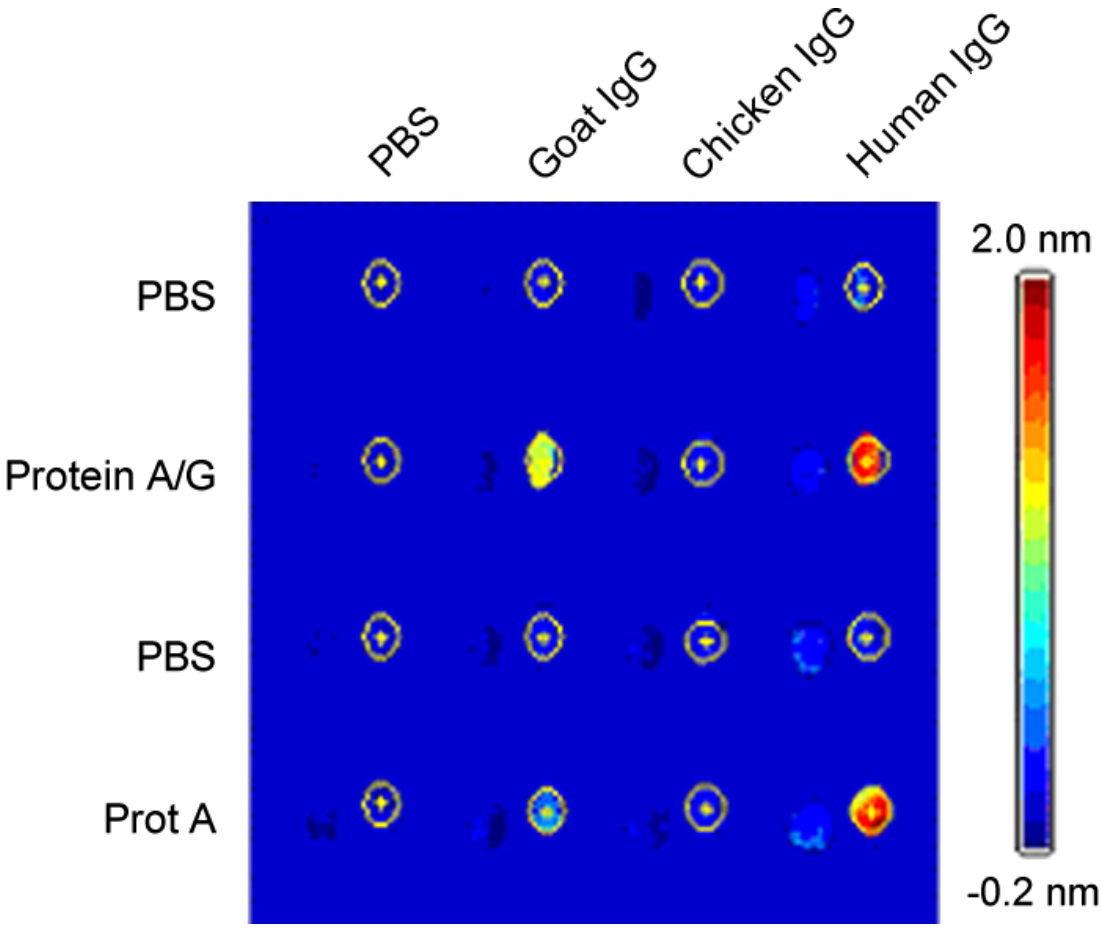

Figure 3.5. The scan results of the proof-of-principle combinatorial screening chip. Two proteins, A and A/G, are tested against Goat, Chicken and Human IgG antibodies. Three rows are reserved as controls, filled with only phosphate buffer solution. The binding results shown here are expected for these protein and antibody combinations.
[Reproduced by permission of The Royal Society of Chemistry (RSC), [18]]

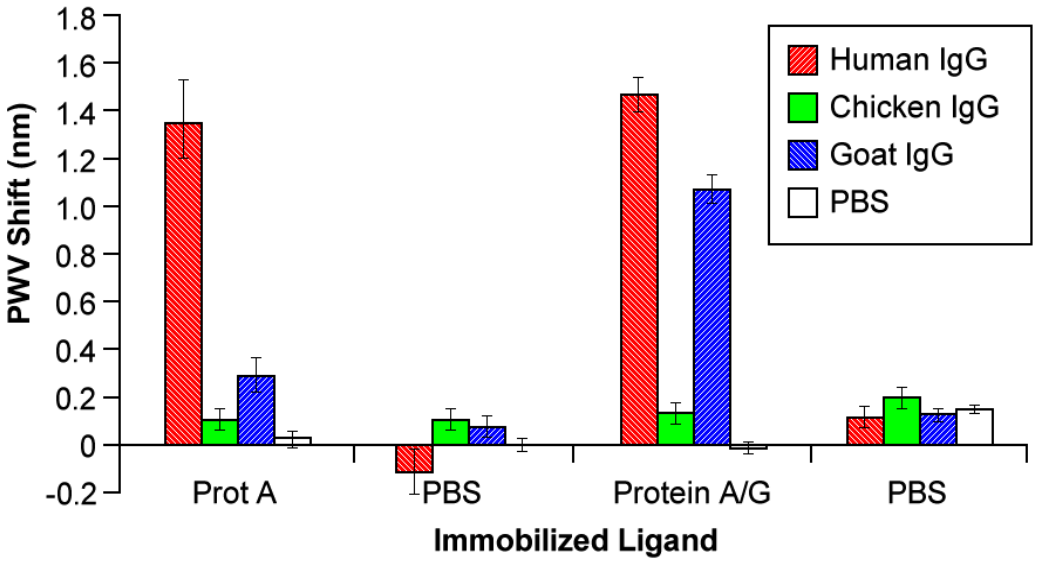

Figure 3.6. A graph of the protein antibody-assay for the proof-of-principle experiment. As expected, human and goat IgG adhere strongly to protein A/G, while only Human IgG adheres strongly to protein A. Chicken IgG does not adhere strongly to these proteins.
[Reproduced by permission of The Royal Society of Chemistry (RSC), [18]]

3.3. Conclusions

The microfluidic combinatorial mixing chip described in this chapter exhibited a low propensity for leaking, despite using only a reversible seal between the microfluidic part and the sensor surface. The successful execution of the proof-of-principle protein-antibody experiment further demonstrated the high fidelity of the chip. Leaking did not appear to interfere with chip operation and function.

Future applications of this work would go beyond the proof-of-principle bind experiment described here. For example, one can envision studying protein targets against libraries of small molecules that are synthesized in situ using click chemistry. The integration of the fine control of the combinatorial screening chip with the sensitivity of the photonic crystal biosensor could be further studied to determine viability in real world drug discovery experiment and analysis.

The demonstration of a combinatorial chip capable of this kind of mixing opens up new possibilities for performing a variety of reactions on top of a given sensor substrate. One such possibility, using fluorescence as a response within a microfluidic chip, is expounded upon in Chapter 4, with the specific purpose of virus detection.

3.4. Materials and Methods

3.4.1. Device Design and Assembly

Devices were prepared in Freehand MX using multilayer soft lithography as discussed in previous work [21, 22]. For designing the combinatorial screening chip, the fluid layer was composed of a network of four horizontal channels intersecting with four vertical channels, each 75 µm in width. At the end of these channels, 600 µm circular regions were designed to make the inlet/outlet ports. The half-well chambers were composed of 250 µm circles connected to 150 µm lines forming the U-shaped half-wells. All gaps for these microchannels were 40 µm in width and placed at an angle whenever possible to reduce the pressure required to open the valves.

The control layer was also designed using Freehand MX. Square valves were placed throughout the device to cover each gap of the fluid layer, measuring 248 µm x 236 µm for the valves over horizontal flowing microchannels, 198 µm x 495 µm for the valves over the vertical flowing channels, and 292 µm x 347 µm for the mixing valves. These valves were connected via 49 µm microchannel runner lines to three input circles, 600 µm in diameter. In order to connect the three types of valves to only three valve inputs, the mixing and the vertical movement valves were interdigitated across the chip, with the horizontal flowing valves snaking back and forth throughout the design.

Because the horizontal valves travel across the farthest length, these valves were the most susceptible to vacuum leakage and were often the first to malfunction if the chip showed signs of failure.

These designs were then replicated onto a transparency mask using the laser printing services of the University of Illinois Print Shop (5080 dpi). Two silicon wafers were first cleaned using acetone and then isopropanol, followed by drying under nitrogen and heated to 110°C to remove any water that might condensate onto the silicon wafers during drying for 10 minutes. At the end of this drying time, the wafers were placed inside a spin coater. Two milliliters of SU-8 25 were placed on the center of the wafer for spin coating treatment. The program run by the spin coater ramped up to 2000 RPMs over 10 seconds, and then held at 2000 RPMs for 30 additional seconds. After this, it ramped back down to 0 RPMs in 10 seconds. This procedure yielded a thin layer of photoresist, approximately25 μm in height.

After coating, the wafer was then placed onto a hot plate preset at 65°C for 4 minutes. The wafer was then transferred to the second hot plate at 95°C for 8 minutes. The wafer was then allowed to cool for 1 minute, and then placed in a collimated UV light source and exposed for 20 seconds at 11 $\mu W/cm^2$. The wafer was then developed in PGMEA (propylene glycol methyl ether acetate) for 5 minutes, taking care to rinse with ispropanol. If any white residue remained on the surface of the silicon wafer, it was placed back in the PGMEA and developed further. When the silicon wafer could be rinsed with isopropanol and no white residue remained, the wafer was subsequently dried under nitrogen and stored in a petri dish. At this point, the silicon wafers with the photoresist designs are to be called masters.

To prepare these masters for device production, they were first placed in a dessicator with silanizing agent for four hours. PDMS monomer and crosslinking agents were mixed in a 5:1 ratio for the control layer, and a 15:1 ratio for the fluid layer. This difference in crosslinker ratio allows for a tighter bond between the two layers after partially curing the layers separately. The very first time a control master is used for device fabrication, 30 g of PDMS mixture will be required to pour into a standard size petri dish, which will yield a device with a thickness around 3-5 mm. Subsequent devices made with the control master will only need 15 g of PDMS, due to the ring of unused PDMS that can be used as a placeholder from earlier device fabrication attempts. For the fluid layer, only 10 g of PDMS mixture is needed. 1-2 mL of PDMS is poured onto the surface of a fluid layer master, which is then placed inside a spin coater for the same program outlined above at 2000 RPMs. This will yield a thickness of 45 µm PDMS for microchannels that are 25 µm in height.

Both layers are placed inside an oven set to 65°C for 30 minutes, and are then checked for tackiness. If the PDMS on the fluid layer master is solid but still sticky, the device can be aligned. The control layer is cut out using a razor or scalpel, and holes are punched to connect to the valves in the control layer. Given that the height of the control channels is only 25 µm, this pattern can be very challenging to see. The use of additional and direct lighting is absolutely required, since any failed punch will destroy the utility of the device. When all holes to the control layer valves have been punched, the fluid layer master is placed onto a vacuum-chuck mount under a microscope. Alignment requires careful placement of the control layer above the fluid layer, while making sure valves align properly to gaps in the fluid layer. This can be done by hand,

or using a mechanical alignment system for careful iterative adjustment. If only a certain portion of the valves are aligned, the device can be lifted at a corner, causing the design to be stretched or contorted to fit all valves onto the fluid layer.

Once the valves are aligned, the device is placed into the oven at 65°C for 1 hour to fully cure the layers together to form an irreversible seal. After curing, the device is cut from the fluid layer master using a scalpel or razor, and holes are punched to provide inlets for the fluid layer microchannels exposed on the bottom of the device. If the device is not to be used immediately, it is placed onto a pre-cleaned glass slide to ensure that no dust particles adhere to the clean microchannel surface underneath.

3.4.2. Integration to Photonic Crystal Biosensor

The photonic crystal biosensors, developed in the laboratory of Dr. Cunningham [23, 24], were patterned to 250 μm circles using a targeted replicated molding process reported by our collaborators. The 250 μm circular sensors were patterned to match the design of the fluid layer of the combinatorial screening chip. After the device is fully cured and all inlet ports are punched, the device is aligned to the patterned photonic crystal biosensor surface, aligned such that each u-shaped half-well is perfectly aligned to one photonic crystal sensor.

3.4.3. Proof-of-Principle Protein-Antibody Experiment

Phosphate buffer solution (PBS) is prepared as a pre-treatment for the combinatorial screening chip. All valves of the chip are activated and the phosphate buffer solution is pulled into the chip using vacuum. Because the chip will evaporate over the 24 hour course of treatment, the entire chip is subsequently submerged into PBS in a petri dish

and allowed to sit for 24 hours to fully incubate all PDMS surfaces within the chip. Over the course of treatment, the chip is checked periodically to ensure that the channels do not dry out over time. Because of this treatment, it is typical that the control valves are filled with PBS buffer as well. This is not desirable, but can be managed with effective vacuum operation during the course of the experiment.

After treatment the valves are tested the next day, ensuring small tenting within each control valve, which is indicative of full operation. After valve tests, the chip can be subsequently used for a protein-antibody experiment.

For all experiments outlined here, protein is prepared in PBS solution and loaded into fluid microchannels in horizontal rows only. IgG antibodies, also prepared in PBS, are loaded into vertical channels. Incubation times for the combinatorial experiment outlined in this chapter were 30 minutes, both for incubation and mixing as reported in previous work [18].

The combinatorial screening experiment used two rows incubated with protein (A and A/G) and two rows used as a control using PBS. In the columns, PBS, Human IgG, Goat IgG and Chicken IgG were placed in the control half-well chambers (right wells). These antibodies within the control chambers would nonspecifically bind to the surface of the photonic crystal biosensor. To determine the difference between antibodies that non-specifically bound to the surface of the control compartment and antibodies that specifically bound to the proteins patterned in the experimental compartment, a background scan was taken with the antibodies only in the control half-well. After the mixing valve was opened and the antibodies were allowed to freely diffuse across to the control surface for 30 minutes, the valves were relaxed back to rest state and the

pressure lines were decoupled from the device. The combinatorial device was scanned once more, and the peak wavelength values were background subtracted. The resulting shifts in the peak wavelength corresponded to the expected binding parameters of the protein-antibody assay [25]. Human IgG bound strongly to the Protein A and Protein A/G patterned circles, and demonstrated a large shift. Goat IgG bound less strongly to both proteins and demonstrated a smaller shift. Chicken IgG, which should not bind to either protein, did not show an appreciable shift. This is an important distinction, since the chicken IgG demonstrated a shift of non-specific binding when compared against an untreated surface as seen in depletion experiments.

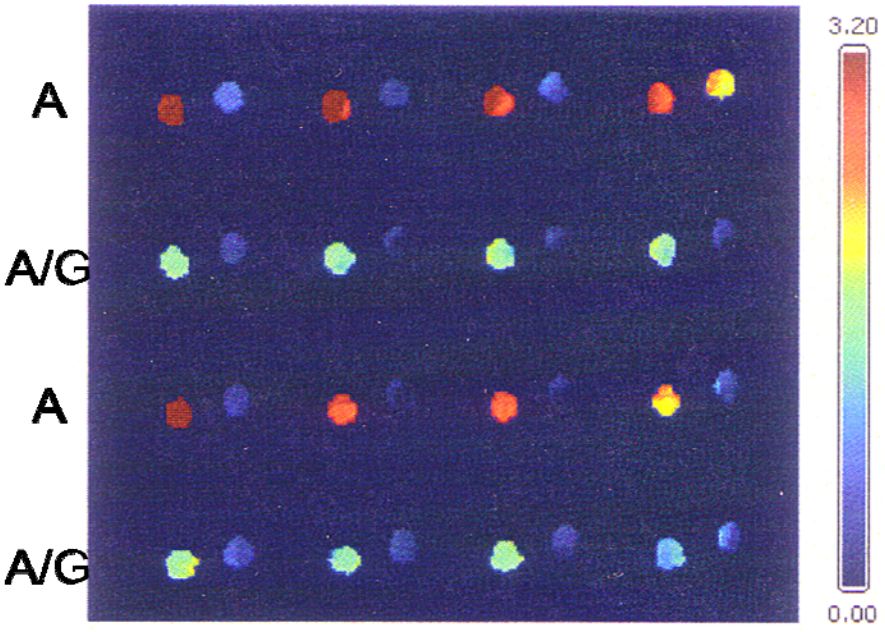

Figure 3.7. A scan of the depletion experiment performed using duplicated rows of protein A and protein A/G. The protein solutions in PBS were incubated in the horizontal rows, which patterned the experiment PC biosensor circles on the left side. A shift of 3.1 nm for the protein A circles indicates a large binding affinity, which is known for that protein. A shift of 1.2 nm for protein A/G is also expected. Flow proceeded from left to right, not showing any decrease in binding.

3.4.4. Depletion Experiments

One of the unpublished results in the combinatorial screening chip experiments was the depletion experiments performed to ascertain the viability of the PC biosensors integrated with the microfluidic mold. A major concern for microreactor studies is how much material is deposited onto microchannels inside the chip rather compared to the amount of material that actually reaches the sensor surface. In order to quantify the effect of depletion, experiments were performed using duplicated protein-antibody experiments on chip.

While in the published data of the previous chip, three lanes of PBS were used as controls to demonstrate a lack of leaking, only one such lane was used as a control for these depletion experiments. Protein A was patterned in two horizontal microchannels, followed by Protein A/G patterned in the other two horizontal microchannels (Figure 3.7). These channels were staggered to ascertain whether protein upstream was being rinsed onto sensors downstream in the IgG loading process, given the serial nature of the chip. A lack of change in color (peak wavelength) from left to right, the direction of flow, indicates that depletion is not a factor in these studies at the concentrations used. Also, since the proteins are duplicated for each set of rows, it would appear that there are few variations across chip.

Subsequently, the antibodies were prepared in PBS and tested in the same way. A single row was selected for control purposes, loading only with PBS (Figure 3.8). For all but one half-well, the IgG showed a propensity for nonspecific binding across only the sensors in the right-hand wells.

In the case of the final half-well on this chip, it was observed that Protein A might have leaked within this well in the previous depletion experiment. Subsequently, the chicken IgG did not show a strong shift in the upper right portion of the well. While this artifact rendered this data unfit for publishing, it is important to note that on occasion the device will exhibit propensity for leaking. Sometimes the cause is observable, such as a dust particle that adhered to the microchannels or sensor surface during fabrication. When a dust particle settles underneath a valve, the particle itself can force the valve to be continually opened and leaking can be observed. It is extremely important for experimental purposes that the device be observed thoroughly, in order to avoid errors of this nature. Because of this leakage in the earlier protein verification experiment, the shift in IgG binding was less in this particular well. In the data published for the proof-of-principle experiment, this issue was resolved [18].

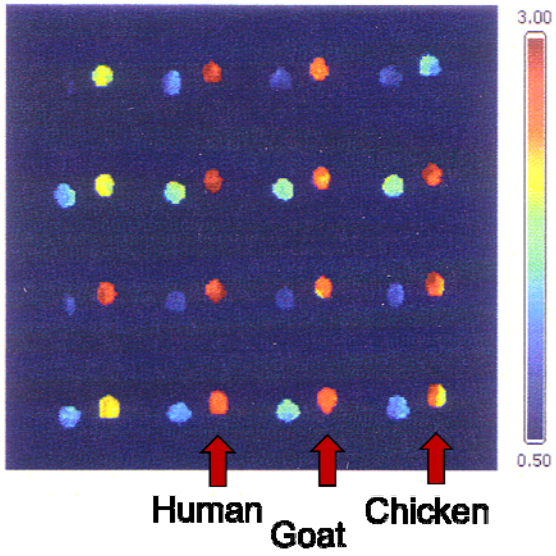

Figure 3.8. A scan of the introduction of IgG antibodies and PBS into the combinatorial screening chip. This scan demonstrates a lack of depletion with flow moving from bottom to top. Also, all sensors show that IgG is only patterning on the right hand side control wells. While the non-specific binding of chicken IgG causes a shift of 2.7 nm as compared to just PBS, this shift is not observed when the chicken IgG nonspecifically binds to the protein during the full experiment.

3.4.5. Protein and Antibody Solutions

Proteins used in the proof-of-principle protein-antibody assay were obtained from Pierce Biotechnology at stock concentrations. Phosphate buffer solution from Sigma-Aldrich was prepared at 0.5 mg/mL. Sea Block from Pierce Technologies was diluted in PBS to 20% by volume. The goat, chicken and human immunoglobulin G (IgG) antibodies were obtained from Sigma-Aldrich and prepared at a concentration of 0.5 mg/mL in PBS. All solutions were stored in a refrigerator at 4°C, prepared from stock solutions that were frozen in a -20°C freezer.

3.5. References

1. Eisenberg, D., E.M. Marcotte, I. Xenarios, and T.O. Yeates, *Protein function in the post-genomic era.* Nature, 2000. **405**(15 June 2000): p. 823-826.
2. Monroy, A.F., F. Sarhan, and R.S. Dhindsa, *Cold-Induced Changes in Freezing Tolerance, Protein Phosphorylation, and Gene Expression (Evidence for a Role of Calcium).* Plant Physiol., 1993. **102**(4): p. 1227-1235.
3. Tegnar, J., M.K.S. Yeung, J. Hasty, and J.J. Collins, *Reverse engineering gene networks: Integrating genetic perturbations with dynamical modeling.* Proceedings of the National Academy of Sciences of the United States of America, 2003. **100**(10): p. 5944-5949.
4. Gygi, S.P., B. Rist, S.A. Gerber, F. Turecek, M.H. Gelb, and R. Aebersold, *Quantitative analysis of complex protein mixtures using isotope-coded affinity tags.* Nature Biotechnology, 1999. **17**: p. 994-999.
5. Fuchs, E., *Keratins as biochemical markers of epithelial differentiation.* 1988. **4**(10): p. 277-281.
6. Darnell, J.E., Jr., *STATs and Gene Regulation.* Science, 1997. **277**(5332): p. 1630-1635.
7. Lipinski, C.A., F. Lombardo, B.W. Dominy, and P.J. Feeney, *Experimental and computational approaches to estimate solubility and permeability in drug discovery and development settings.* Advanced Drug Delivery Reviews, 1997. **23**(1-3): p. 3-25.
8. Carlson, H.A. and J.A. McCammon, *Accommodating Protein Flexibility in Computational Drug Design.* Molecular Pharmacology, 2000. **57**(2): p. 213-218.

9. Lin, J.-H., A.L. Perryman, J.R. Schames, and J.A. McCammon, *Computational Drug Design Accommodating Receptor Flexibility: The Relaxed Complex Scheme.* Journal of the American Chemical Society, 2002. **124**(20): p. 5632-5633.

10. Gordon, E.M., R.W. Barrett, W.J. Dower, S.P.A. Fodor, and M.A. Gallop, *Applications of Combinatorial Technologies to Drug Discovery. 2. Combinatorial Organic Synthesis, Library Screening Strategies, and Future Directions.* Journal of Medicinal Chemistry, 1994. **37**(10): p. 1385-1401.

11. Hann, M.M., A.R. Leach, and G. Harper, *Molecular Complexity and Its Impact on the Probability of Finding Leads for Drug Discovery.* Journal of Chemical Information and Computer Sciences, 2001. **41**(3): p. 856-864.

12. Drews, J., uuml, and rgen, *Drug Discovery: A Historical Perspective.* Science, 2000. **287**(5460): p. 1960-1964.

13. Martin, E.J., J.M. Blaney, M.A. Siani, D.C. Spellmeyer, A.K. Wong, and W.H. Moos, *Measuring Diversity: Experimental Design of Combinatorial Libraries for Drug Discovery.* Journal of Medicinal Chemistry, 1995. **38**(9): p. 1431-1436.

14. Weissleder, R. and V. Ntziachristos, *Shedding light onto live molecular targets.* Nat Med, 2003. **9**(1): p. 123-128.

15. Zernov, V.V., K.V. Balakin, A.A. Ivaschenko, N.P. Savchuk, and I.V. Pletnev, *Drug Discovery Using Support Vector Machines. The Case Studies of Drug-likeness, Agrochemical-likeness, and Enzyme Inhibition Predictions.* Journal of Chemical Information and Computer Sciences, 2003. **43**(6): p. 2048-2056.

16. Rogawski, M.A., *Molecular targets versus models for new antiepileptic drug discovery.* Epilepsy Research, 2006. **68**(1): p. 22-28.

17. Kuhn, P., K. Wilson, M.G. Patch, and R.C. Stevens, *The genesis of high-throughput structure-based drug discovery using protein crystallography.* Current Opinion in Chemical Biology, 2002. **6**(5): p. 704-710.

18. Schudel, B.R., C.J. Choi, B.T. Cunningham, and P.J.A. Kenis, *Microfluidic chip for combinatorial mixing and screening of assays.* Lab on a Chip, 2009. **9**: p. 1676.

19. Choi, C.J. and B.T. Cunningham, *Single-step fabrication of photonic crystal biosensors with polymer microlfuidic channels by a replica molding process.* Lab on a Chip, 2006. **6**: p. 1373-1380.

20. Akerstrom, B., T. Brodin, K. Reis, and L. Bjorck, *Protein G: a powerful tool for binding and detection of monoclonal and polyclonal antibodies.* J Immunol, 1985. **135**(4): p. 2589-2592.

21. Unger, M.A., H.-P. Chou, T. Thorsen, A. Scherer, and S.R. Quake, *Monolithic Microfabricated Valves and Pumps by Multilayer Soft Lithography.* Science, 2000. **288**(5463): p. 113-116.

22. Thorsen, T., S.J. Maerkl, and S.R. Quake, *Monolithic Microfabricated Valves and Pumps by Multilayer Soft Lithography.* Science, 2002. **298**: p. 580-584.

23. Block, I.D., L.L. Chan, and B.T. Cunningham, *Photonic crystal optical biosensor incorporating structured low-index porous dielectric.* Sensors and Actuators B-Chemical, 2006. **120**(1): p. 187-193.

24. Block, I.D., L.L. Chan, and B.T. Cunningham, *Large-area submicron replica molding of porous low-k dielectric films and application to photonic crystal biosensor fabrication.* Microelectronic Engineering, 2007. **84**(4): p. 603-608.

25. Heitzmann, H. and F.M. Richards, *Use of the Avidin-Biotin Complex for Specific Staining of Biological Membranes in Electron Microscopy.* Proceedings of the National Academy of Sciences of the United States of America, 1974. **71**(9): p. 3537-3541.

Chapter 4

Total Internal Reflection Fluorescence Microscopy-based Combinatorial Screening

4.1. Introduction

The photonic crystal biosensor described in Chapter 3 is ideal for proteins or other large molecule (kilodalton) binding experiments. But for smaller compounds such as single stranded DNA in viruses, other routes can be advantageous. In particular, fluorescence microscopy is an excellent candidate to probe interactions with nucleic acids, facilitated by the large number of chemical alterations that can be performed with DNA labeled with fluorescent markers [1]. For this study, DNA hybridization is studied in a multiplexed fashion using the combinatorial screening chip discussed in Chapter 3. Because the device uses AtO valves which require a reversible seal to the bottom layer, a wide variety of sensors can serve as the bottom substrate of the microfluidic device. For virological studies of nucleic acids, molecular beacons can be used to observe fluorescence in the presence of the genetic material of a virus, sensing at concentrations lower than conventional virology methods [2]. In this work, molecular beacons are studied in a combinatorial screening chip for multiplex detection of viral targets using total internal reflection fluorescence (TIRF) microscopy.

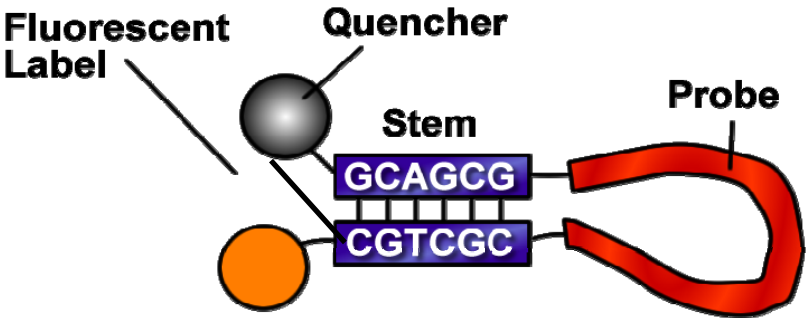

Figure 4.1. Schematic of a molecular beacon. A fluorescent label and quencher pair are attached to opposite ends of a single strand of DNA. The first and last 6-8 DNA bases are G-C rich and complementary, forming a stable bond. The 20-base probe region is complementary to a DNA target oligonucleotide, which causes the beacon to open upon hybridiziation.

4.1.1. Molecular Beacons

Molecular beacons, proposed and studied by Tyagi *et al.*, are single-stranded DNA probes with a self-complementary stem region occurring in the first and last 6-8 bases [3]. They are designed to fluoresce in the presence of a complementary single-stranded DNA target oligonucleotide. In the absence of the complementary oligonucleotide, these molecular beacons exist in a dark state due to dye quenching [4-6].

A fluorescent dye and quencher pair are attached at opposite ends of the complementary stems, which quenches fluorescence when the beacon exists in a hairpin conformation (Figure 4.1). The internal 20-base section of the DNA is the probe region, which is complementary to a target DNA strand such as the genetic material in a single stranded virus. In the presence of the viral DNA or RNA, the beacon will hybridize to the target oligonucleotide and change conformation to an open state, thereby forcing the quencher and fluorescent labels apart such that the fluorescence emission from the dye molecule can be detected (Figure 4.2). The hybridization can be performed at room temperature or amplified in temperature ramp cycles during PCR [7].

Due to the exquisite specificity of DNA base pair binding, molecular beacons are highly sensitive, capable of distinguishing between a perfect match and single base mutants [3]. As such, these beacons are ideal candidates for very sensitive detection of low concentration DNA such as virus genetic material that may occur in concentrations too low to detect by conventional means [7]. In experiments, the fluorescence signal detected by a camera or imaging device includes non-specific sources of fluorescence from ill-formed molecular beacons, foreign organic matter, and the intrinsic fluorescence of the material of the device, all of which increase the fluorescence background signal during the experiment. In order to achieve a higher signal to noise ratio, the background fluorescence will need to be reduced. In this work, a technique known as total internal reflection fluorescence (TIRF) microscopy enables detection in a small region adjacent to the surface where fluorescent markers are specifically immobilized, which allows for determination of target oligonucleotides containing viral genetic sequences.

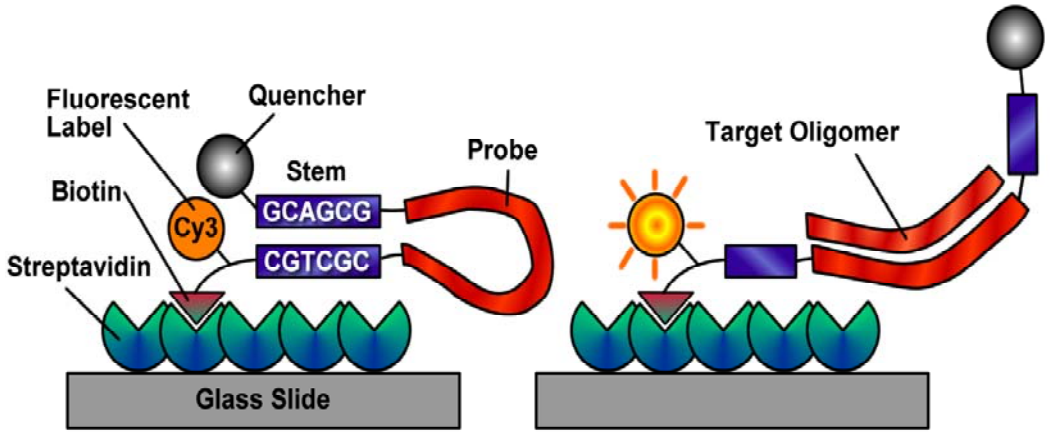

Figure 4.2. A schematic of the molecular beacons specifically linked to a glass slide. BSA-biotin is patterned onto a glass surface, followed by streptavidin. BSA is then used to nonspecifically block any remaining binding sites on glass. The biotinylated molecular beacon is incubated onto the streptavidin and remains in the quenched state on the surface. In the presence of the complementary matching target oligonucleotide, the beacon will fluoresce on the surface.

4.1.2. Total Internal Reflection Fluorescence Microscopy

Total internal reflection fluorescence (TIRF) microscopy (Figure 4.3) is used to generate a small fluorescence excitation volume in the vicinity of the surface, thereby exciting only sample materials specifically linked to the surface [8-10]. By excluding fluorescent material away from the surface, signal is not artificially increased from external factors, such as PDMS [11, 12]. TIRF microscopy differs from epifluorescence microscopy, where material in solution or otherwise far from the glass surface may contribute to the fluorescence signal, which results in high background.

In using TIRF microscopy, the molecular beacons must be linked directly onto the microscope coverslip. This chemical linkage is achieved using biotoin and streptavidin linkages. DNA molecular may be purchased with a wide variety of chemical modifications including fluorescent labels [1, 13-16], surface chemistry linkers [17-21] and spacers [22-25] within the DNA chain. The wide array of DNA modification chemistry that can be performed also provides for a surface-based modification of the molecular beacons mentioned above. For this study, biotinylated beacons [26] were synthesized by Integrated DNA technologies Technologies with a fluorescent label HEX (hexachlorofluoroscein) and a quencher (Iowa Black) component, with a biotin component located internally within the DNA along the stem [27, 28]. Molecular beacons are then specifically linked onto a glass coverslip using surface chemistry protocol discussed in Section 4.4.3.

The main advantage in using a surface based approach is the degree of control that can be implemented during loading of the microchannels with molecular beacons

modified with various chemical functionalities. For sensitive experimental analysis of a low concentration analyte, surfaces can be loaded with extremely low concentrations of molecular beacons down to the limit of single molecules. Alternately, experiments may also be conducted with high-concentration loading of bound molecular beacons. Following a beacon binding to the surface, excess unbound fluorescent material is rinsed away with buffer. A precisely loaded concentration of fluorescent beacons remains on the surface, controlled by the loading concentration buffer and the duration of incubation. Overall, this protocol can be used for studies in glass-based flow cells and in the PDMS-based combinatorial screening chip discussed in Chapter 3.

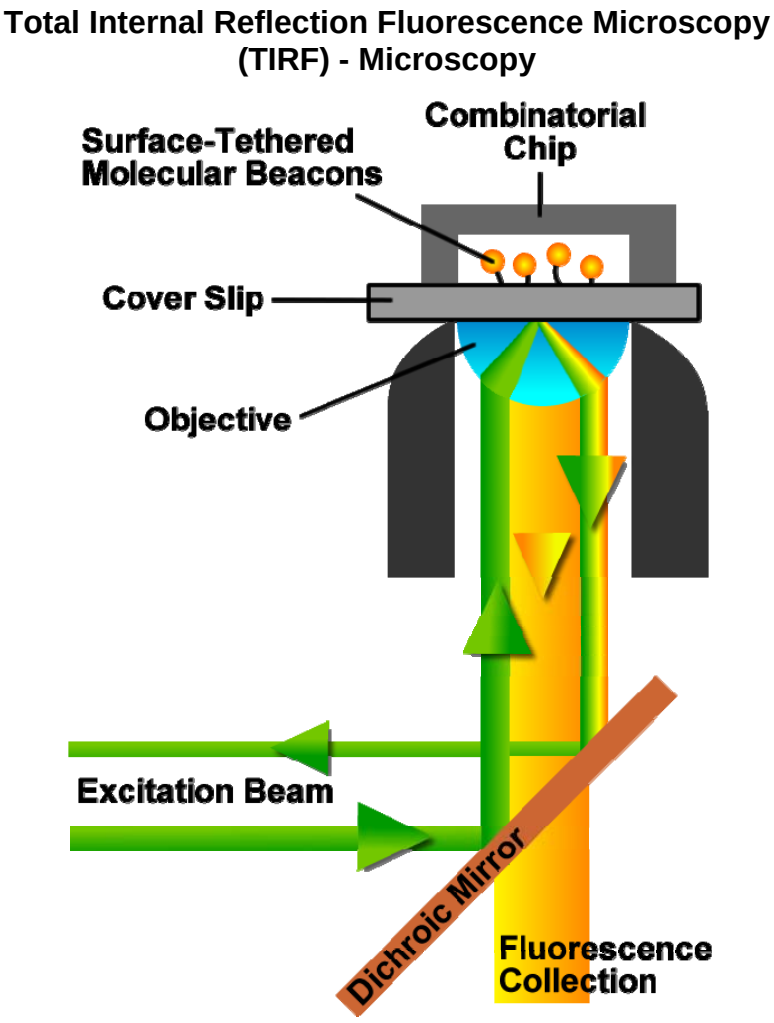

Figure 4.3. In total internal reflection fluorescence (TIRF) microscopy, the excitation beam enters the microscope and is directed onto the objective lens upon reflection off of the dichroic mirror. This beam then impinges on the glass coverslip at an angle through immersion oil. The beam impinges on the coverslip at an incident angle greater than a critical angle for total internal reflection, generating an evanescent wave into the medium of the sample above the glass. As such, excitation only occurs within ~100 nm of the region above the coverslip. The excitation fluorescence is then collected as the beam passes through the dichroic mirror and is captured by a fluorescence camera.

4.2. Results and Discussion

4.2.1. "Bulk" Well Plate Studies of Molecular Beacons

To establish the bulk detection sensitivity of the molecular beacons, concentration variation experiments were performed in 96-well optical microplates at the 50-100 µL

scale. Measurements were first performed using PJAK-1 and PJAK -2 molecular beacons (Table 4.1) at varying concentrations in epifluorescence detection in a microplate reader. Experiments were conducted both with (signal) and without (background) complementary target oligonucleotide present in a variety of concentrations. The difference between signal and background is the signal to noise ratio, which will be crucial in ascertaining if the beacons are viable at extremely low concentrations.

4.2.1.1. Background Fluorescence

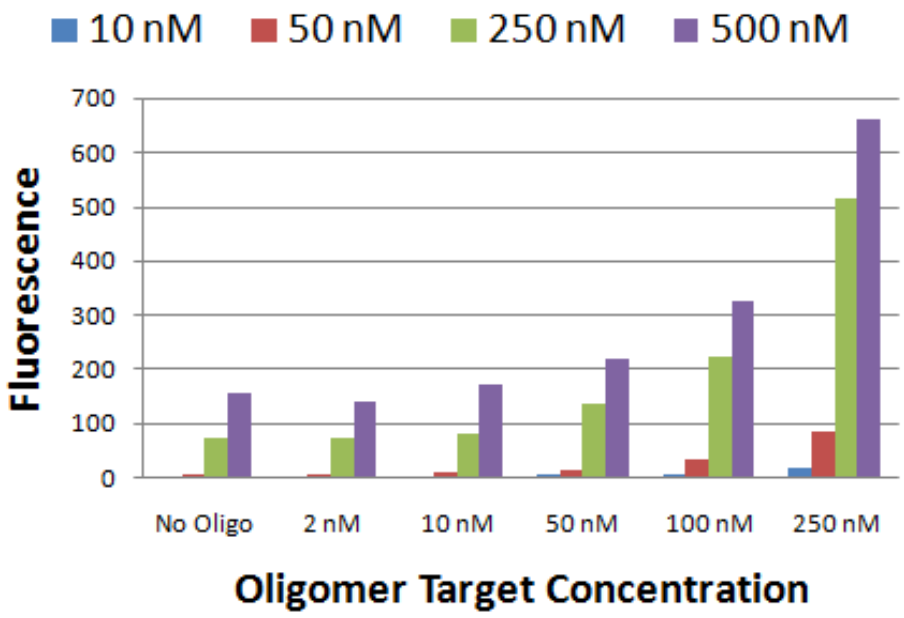

Figure 4.4. Plot of fluorescence signal from binding studies using molecular beacon PJAK-2 loaded in a microplate reader at volumes of 100 µL per experiment. In each well, a final concentration of complementary target oligonucleotide of 0, 2 nM, 10 nM, 50 nM and 100 nM were added to the solution and mixed for 1 hour. The final result shows the molecular beacon fluorescence both for the background (No Oligo) and in the presence of different concentrations of the target oligonucleotide. This data indicated a sensitivity limit on the order of 10 nM oligomer concentration, below which the signal is indistinguishable from background.

Figure 4.4 shows the fluorescence detected in binding studies of the molecular beacons at concentrations between 10 nM and 500 nM for the PJAK-2 beacon mixed with the complementary target oligonucleotide cPJAK in concentrations between 0 and 250 nM. In epifluorescence measurements, the background (with no target oligonucleotide present) has a similar response to the 2 nM and 10 nM regimes. Previous work has indicated a sensitivity limit of ~2 nM for other molecular beacons in flow cytometry [29], which is approximated as similar to the limit observed in this work at the bulk concentration level. However, the sensitivity limit is likely a function of nucleic acid sequence.

Molecular beacons may show a lower sensitivity limit, particularly when coupled to microscopy techniques due to the amplification of signal. A possible explanation is that the beacons may exhibit intermolecular interactions at higher concentrations [29]. Beacons can self-hybridize and transition to an open conformation. One way to circumvent this problem is to utilize surface-bound becaons. After beacons are specifically linked to a surface, additional beacons or fluorescent material can be rinsed away by buffer exchange. Also, specific chemical linkage of beacons prevents detection of fluorescent particles diffusing in solution.

4.2.1.2. Kinetic Response

Figure 4.5 shows the kinetic fluorescence response of molecular beacons binding to target oligonucleotide as a function of time. Four concentrations of molecular beacon PJAK-2 were loaded into a microplate at volumes at 50 µL of 0 nM, 50 nM, 250 nM and 1.25 µM. An additional 50 µL of complementary target oligonucleotide cPJAK was

added to each of the wells at concentrations of 0 nM, 100 nM, 500 nM and 2.5 μM. Solution in the wells was mixed by pipette and then subsequently scanned in a microplate reader, which acquired data at the rate of one measurement per minute for 70 minutes.

Over the course of 1 hour, fluorescence counts increased as expected for a bimolecular reaction. At time scales as low as 10 minutes, the target oligonucleotide signal is over ten times the background signal (Figure 4.5). This would indicate that a sufficient duration for the molecular beacons to hybridize is 10 minutes, assuming the solutions are well-mixed. Given that the mixing capabilities of our combinatorial screening chip are diffusion limited as observed in Chapter 3, this indicates the combinatorial screening experiment should allow 1 hour at most for both proper mixing and surface hybridization to occur.

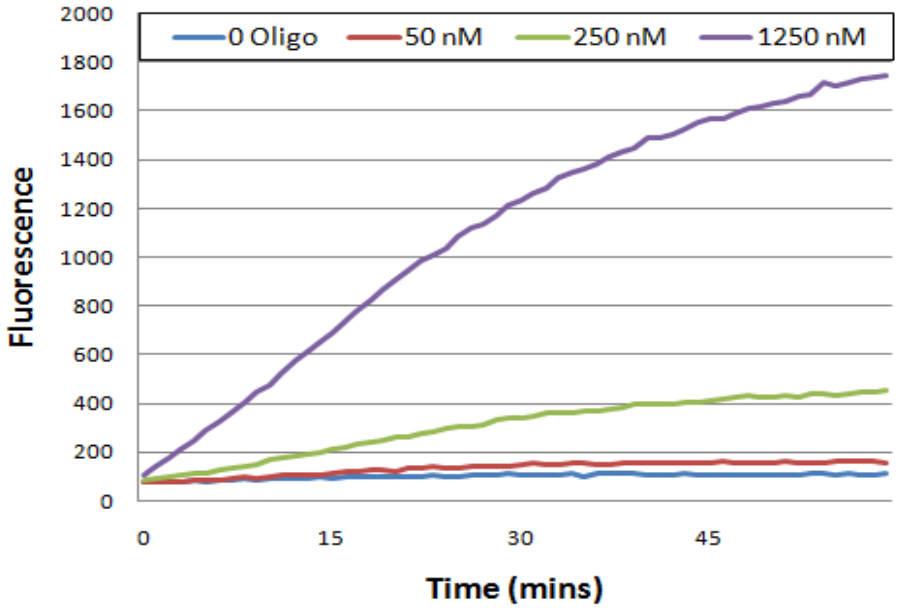

Figure 4.5 A graph of the kinetic fluorescent response of molecular beacon PJAK-2 (250 nM) to target oligonucleotide. Four wells in a microplate had four concentrations of target oligonucleotide mixed by pipette at t=0. Fluorescence readings were acquired once per minute within each well over the course of 70 minutes. Within as little as 10 minutes, a fluorescent signal ten times as large as the background baseline can be observed.

4.2.1.3. Viability of Specifically Linked Molecular Beacons

To validate the surface modification chemistry of the molecular beacons, an experiment was performed within a microplate at the 50-100 µL scale (Figure 4.6). For the three-step preparatory process for glass surface chemistry modification within a microplate (discussed in Section 4.4.3.), each step of the surface chemistry modifications were included (+) or not included (-). The three steps were: BSA-biotin treatment for 15 minutes, Neutravidin treatment for 15 minutes and BSA for 15 minutes. For each well, a fluorescence measurement was made for (i) the 250 nM molecular beacons in solution (beacon background in solution), (ii) the glass surface rinsed after the 250 nM molecular beacons were loaded (beacons on surface under buffer) and (iii)

with target oligonucleotide introduced into the solution (beacons on surface under oligomer).

The first result in Figure 4.6 shows that when all three surface chemistry steps are utilized, beacons remain viable and increase in fluorescence when the complementary target oligonucleotide is added. In fact, the surface chemistry modifications indicate that Neutravidin alone is sufficient for the molecular beacons to function. For the four wells in which Neutravidin was used, the beacons bound to the bottom surface and were active in solution. For the four wells without Neutravidin, the beacons did not specifically link to the surface and were subsequently rinsed out of the chambers. In the remainder of the experiments discussed in this thesis, all steps are generally utilized, as the data indicates that the beacons remain chemically viable and able to hybridize to the target oligonucleodies when specifically linked to the surface.

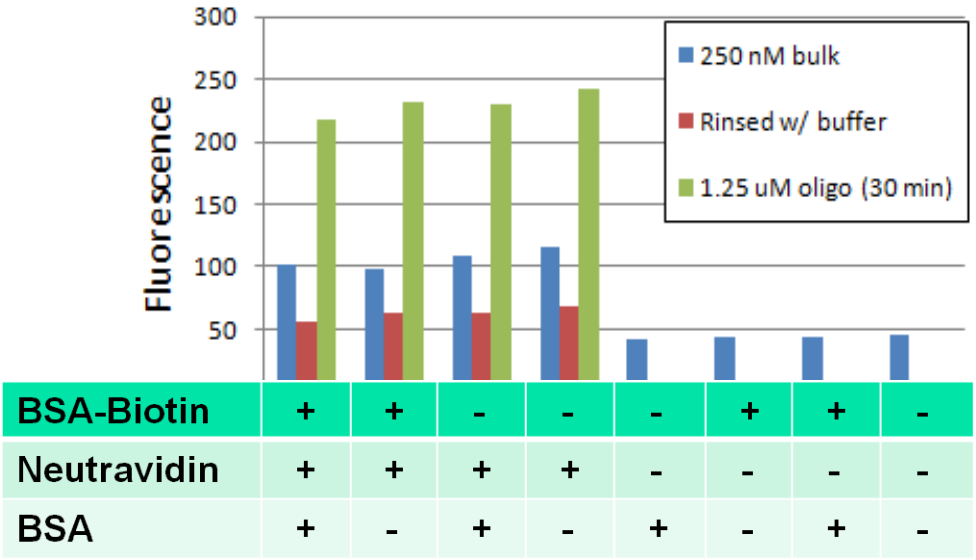

Figure 4.6. A graph of the fluorescence response of PJAK-2 in wells with beacons loaded on the surface, rinsed out, and finally treated with complementary target oligonucleotide. The surface treatment including neutravidin appears to be the only sufficient condition for beacon response.

4.2.2. Fluorescence Measurements in Flow Cells

Glass flow cells were constructed using glass coverslips and two-sided tape as indicated in Section 4.4.4. Each flow cell was loaded with BSA-biotin, neutravidin and BSA. Subsequently, molecular beacons at 250 nM concentration were loaded into the flow cells and allowed to incubate for 1 hour and then rinsed with TE 50 buffer. Fluorescence signals were detected by mounting the flow cells onto a microscope stage and fluorescence signals were collected using a charge coupled device (CCD) camera (Andor Solis).

Initial observation of the flow cells showed a high fluorescence background as compared to the signal (Figure 4.7). Although background comparisons of the microplate reader showed a signal to noise ratio of 5:1, the signal observed in glass flow cells appear to be closer to 1.2:1. It is possible that loading concentrations are much higher in glass based flow cells, due to the surface area to volume ratio typical of microfluidic channels. For the combinatorial experiments for multiplexed virus detection, the sensitivity limit for these beacons may need to be lowered in order to reduce overcounting and/or overcrowding on a glass surface.

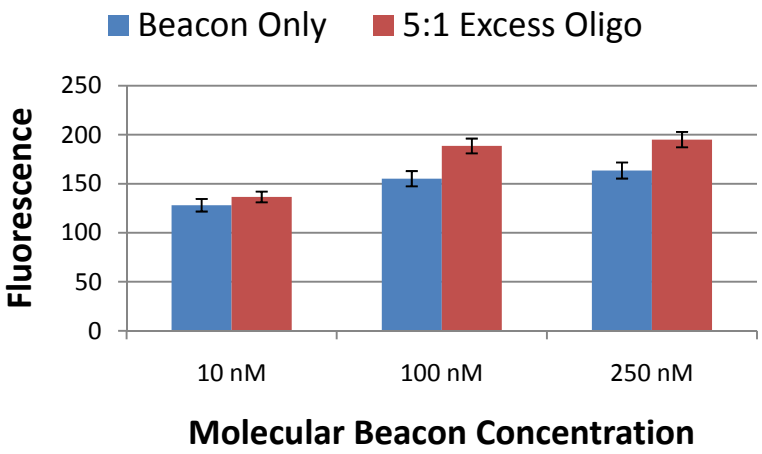

Figure 4.7 A graph of PJAK-1 molecular beacon fluorescence response in glass flow cells. For all three tested concentrations (10, 100 and 250 nM), a small but measurable increase in the fluorescence response was observed when exposed to the complementary target oligonucleotide in 5:1 ratios.

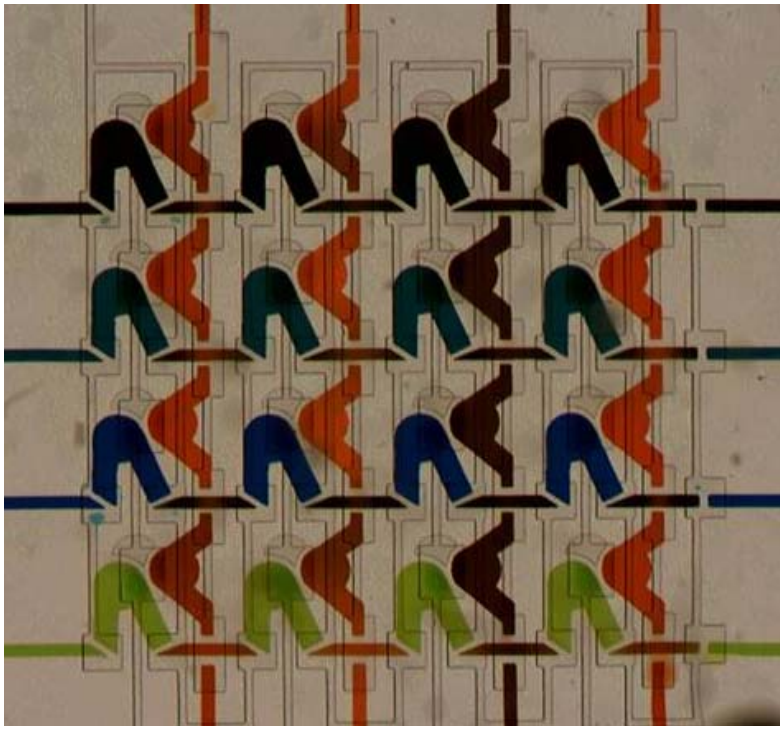

Figure 4.8 An optical micrograph of the fluid layer of the combinatorial screening chip, described in Chapter 3. Four rows save four 200 pL plugs, sealed by passively closed Actuate-to-Open valves. After these plugs are conserved, four columns perform the same way to create a matrix of 4 x 4 combinations. In molecular beacon experiments, the rows are used for different molecular beacons, while the columns are used for the virus-representative samples.

4.2.3. Multiplexed Viral DNA Detection

Four molecular beacons containing a HEX and Iowa Black fluorescent and quencher pair were obtained from commercial vendor Integrated DNA Technologies (IDT, Table 4.1). Each beacon was specifically designed to contain the complementary sequence of HIV, HPV and Hepatitis A and Hepatitis B. Oligomer samples representing conserved regions of each of the genetic material of each of the genes of these viruses previously identified in literature were used as the representative samples of the target viruses [2, 30-32].

Name	**Sequence**
PJAK-1	#CCACGGTAAGTGTCGTCAACCCGTGG$
PJAK-2	#GCAGCGTAAGTGTCGTCAACCGC**T***\GC$
HIV	#CGTCGCAGTACTCACCAGTCGCCGCCCCTCGCCC**T***\GCGACG$
HPV	#CGTCGCAGAAAACCAGTTGTGTCCAAAGGTGTCAGCC**T***\GCGACG$
HepA	#CGTCGCAGGGATAGGGTAACAGCGGCGGCC**T***\GCGACG$
HepB	#CGTCGCAGGGCTTTCAGTTATATGGATGCC**T***\CGCACG$
cPJAK	GTTGACGACTCTA
cHIV	GGCGAGGGGCGGCGACTGGTGAGTA
cHepA	CCGCCGCTGTTACCCTATCC
cHepB	CATCCATATAACTGAAAGCC
cHPV	CTGACACCTTTGGCACAACTGGTTTT

Table 4.1 A table of sequences for the six molecular beacons and the corresponding target oligonucleotides. # represents a 5' HEX modification, **T*** represents a biotinylated linker attached to the T-base within the stem, and $ represents the Iowa Black quencher attached to the 3' end. Probe regions within the beacons are highlighted in grey, and are complementary to the target oligonucleotides used in this studied, prefaced by the letter c.

For the combinatorial mixing chip, four beacons were introduced at 100 pM concentrations within each row for each of the viruses using the surface chemistry modifications outlined in Section 4.4. After 30 minutes of incubation, the rows of beacon solution were rinsed out with imaging buffer containing 0.04% β-D glucose, 2%

catalase and 2% glucose oxidase to minimize photobleaching during the 1-hour multiplexed experiment.

Within each of the columns, target oligonucleotides at 100 nM concentration was introduced. The chip was then mounted onto the fluorescence microscope, and the incoming excitation beam was directed to beacons on the surface in TIRF. For background measurements, three regions of interest were selected within each well and 20 images were collected within each region over 10 seconds at an exposure time of 500 milliseconds. After the background was taken, the chip was transported to a vacuum source, and the mixing valves were actuated to allow the individual target oligonucleotides to diffuse to the beacon loaded compartments. After allowing 30 minutes for diffusional mixing, the chip was again mounted onto the fluorescence microscope and data was acquired in three different regions of interest.

As shown in Figure 4.9, only the perfect match beacon-target oligonucleotide combination yielded the highest fluorescence response. Fluorescence signals showed standard deviation of ± 100 counts, which represents a statistically significant validation of the molecular beacon chip for multiplex virus detection. Overall, this indicates the microfluidic chip is an excellent method for determining the prescence of viral genetic material in a series of half-wells on-chip using very low (200 pL) amounts of material.

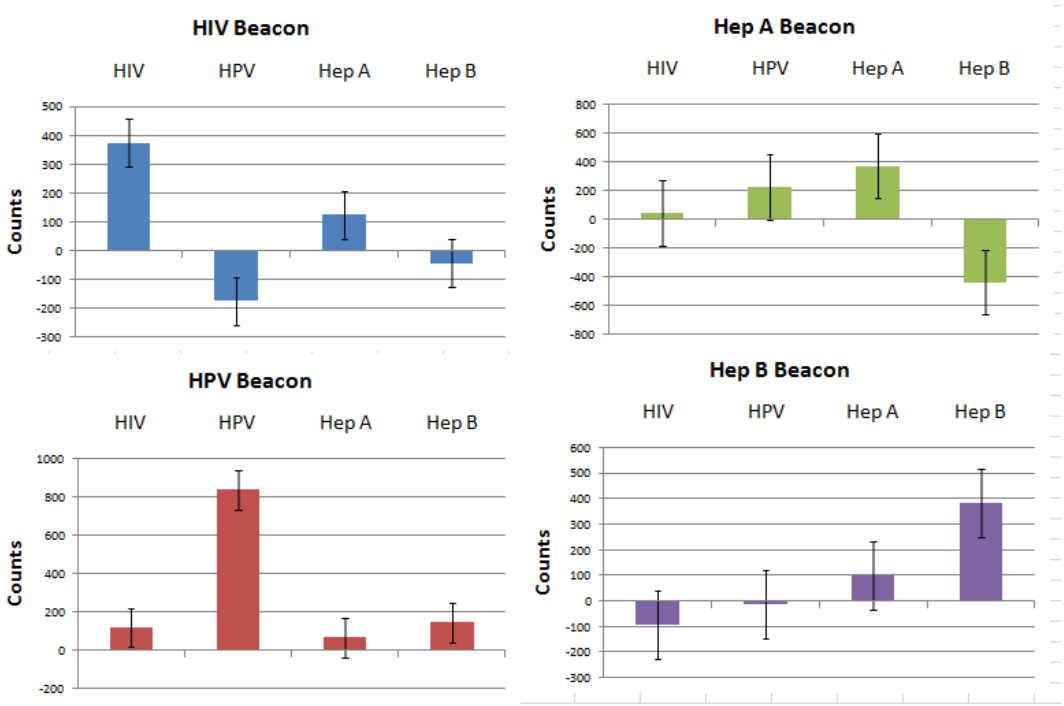

Figure 4.9 Plots of fluorescence measurements for beacons loaded on the combinatorial microfluidic mixing and screening chip. Each beacon is tested against the four oligomer targets, and the strongest response from each beacon corresponds to its perfect match. Negative values (HIV Beacon - HPV Target, Hep A Beacon to Hep B target oligonucleotide) may be due to fluorescent particles artificially raising background, or due to photobleaching on chip.

Name	**Sequence**
PJAK-1	#CCACGGTTGTGGGTCAACCCCGGTGG$
PJAK-2	#GCAGCGTAGAGTCGTCCAACCGC**T***\GC$
cPJAK	GGGGTTGACCCACAAG
cPJAK-O1	GGGGTTCACCCACAAG
cPJAK-O2	GGGGTTCACCGACAAG
cPJAK-O3	GGGTTTCACCCGACAAG

Table 4.2. A table of sequences for the two molecular beacons and the corresponding target oligonucleotides. # represents a 5' HEX modification, **T*** represents a biotinylated linker attached to the T-base within the stem, and $ represents the Iowa Black quencher attached to the 3' end. Probe regions within the beacons are highlighted in grey, and are complementary to the target oligonucleotides used in this studied, prefaced by the letter c. These beacons, modified with 1, 2 or 3 mutations, are underlined to emphasize the mutation placement.

The molecular beacons studied in this work are capable of distinguishing target oligonucleotides with single or multi-base changes in sequence. Virus identification can

be challenging, as viral genetic material has the ability to mutate in the replicative process [33-36]. Identifying not only the presence of a virus, but also possible mutants based on fluorescence detection, would be extremely advantageous for point-of-care multiplex screening. Molecular beacons have previously been studied for mutant detection, but were limited to temperature variations to melt apart the mutant-DNA mismatches [3]. To determine the sequence specificity of the molecular beacons, PJAK-2 molecular beacon was examined at room temperature using four different target oligonucleotide samples with a varying number of mutants (Table 4.2).

The molecular beacon sensitivity to the number of single base mismatches in the target sequence was first examined using a microplate reader. In this experiment, 50 µL of 250 nM of PJAK-2 was introduced into each of five wells in an optical microplate. Within each of these chambers, a corresponding target oligomer with 0, 1, 2, or 3 base mismatches was introduced into each chamber at a final concentration of 1.25 µM. The fluorescence response was then measured once per minute for 60 minutes. Figure 4.10 demonstrates that the molecular beacon sensitivity is entirely dependent on the number of mismatches, and the beacons can clearly distinguish between 1, 2, 3, and no base mismatches.

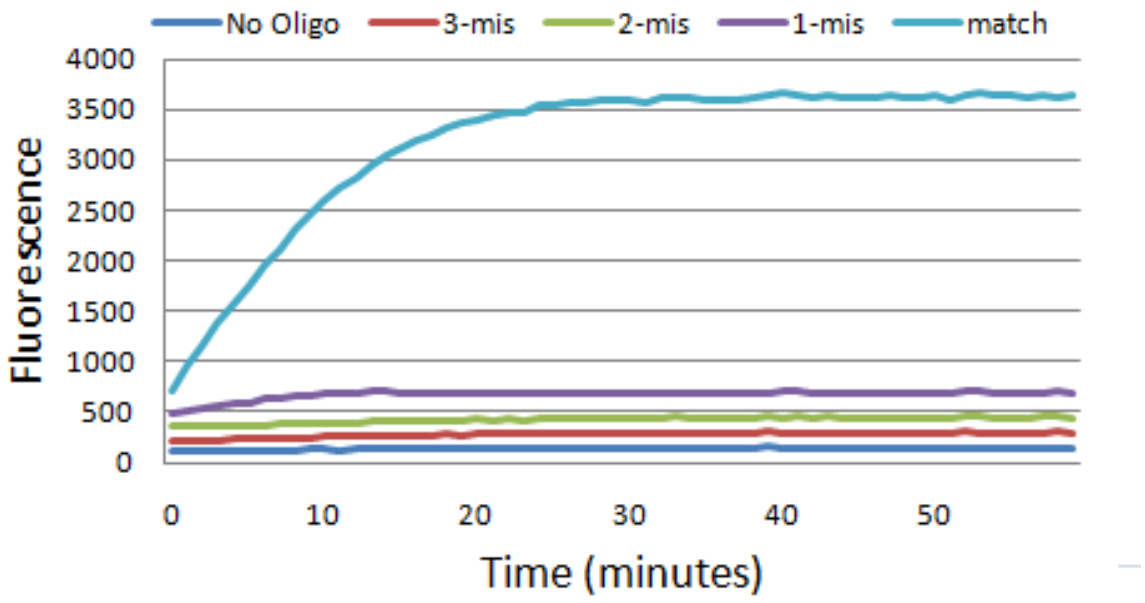

Figure 4.10. A plot of the fluorescence response (arbitrary units). Five wells in a microplate were loaded with 250 nM molecular beacons. Target oligomers with 0, 1, 2, and 3-mismatched bases were introduced at a concentration of 1.25 μM into four of the wells at a total volume of 100 μL. The fluorescence readout was sampled every minute for 60 minutes. During the course of the experiment, the beacon fluorescence response was based entirely on number of mismatches.

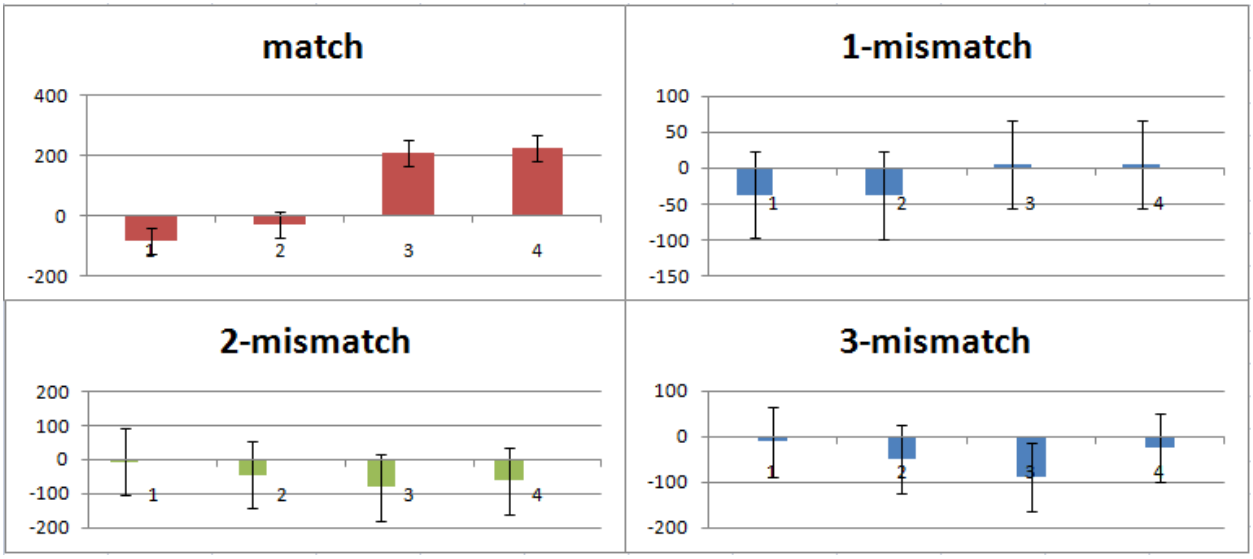

Figure 4.11. A plot of the background-subtracted fluorescence response in arbitrary units for the PJAK-2 beacon against four different target oligonucleotides, segregated by match. For each of the rows, a different concentration of molecular beacon was incubated over the prepared glass surface of the combinatorial device. (1 = 125 nM loading of molecular beacon, 2 = 250 nM loading, 3 = 500 nM loading, and 4 = 1000 nM loading). For all cases except the perfect match at the two highest concentrations of beacon loading, no well indicated an appreciable increase in signal over the background concentration.

The combinatorial screening chip was then employed to study mutant detection using four different concentrations of the PJAK-2 molecular beacon. For each of four rows (1-4), PJAK-2 molecular beacons were incubated at concentrations of 125 nM, 250 nM, 500 nM and 1000 nM for 30 minutes in each row, respectively. Along the vertical wells, 1.25 μM of cPJAK, cPJAK-O1, cPJAK-O2, and cPJAK-O3 were introduced representing the match, 1-mismatch, 2-mismatch and 3-mismatch targets. Surfaces were prepared using the method discussed in Section 4.4.3. The purpose of this experiment was to observe if the results observed in the microplate reader could be replicated at the microscale.

Figure 4.11 demonstrates that only the high concentration trials of 500 nM and 1000 nM PJAK-2 beacons were able to reliably indicate the presence of the matching target oligomer cPJAK. Mutant detection was not possible at the loading concentrations attempted in this work. It is possible that the fluorescent signal would be stronger using imaging buffer to reduce fluorescence variation and photobleaching, but this was not done in this work.

4.3. Conclusions

The combinatorial screening and mixing chip was validated with the molecular beacon experiment for multiplex detection on a 4 x 4 sample for 16 combinations of 4 matches and 12 non-matches. At the low concentration of 100 pM, beacons loaded in each well served as a positive indicator of the presence of a target oligonucleotide containing the conserved sequence of viral DNA. In addition, these experiments utilized

far less molecular beacons than those in previous studies. As a proof-of-principle experiment, molecular beacons function effectively within the combinatorial chip and serve as a viable means of target oligonucleotide detection.

While this work attempted to incorporate mutant detection into the overall scheme of device operation and initial studies using microplate readers indicated the sensitivity of molecular beacons to single base mutant was possible, this level of discrimination was not observed at the microfluidic scale. It is possible that photobleaching could have occurred during the experiment, and future work should utilize an imaging buffer as outlined in the previous example in order to determine if the signal is appreciably strong.

One possible direction would be to begin studying whole viral genomic DNA in a PCR amplification reaction in order to increase the signal to noise ratio. There are a number of hurdles associated to working with live viruses including biosafety protocols and mutations, which would have to be circumvented in order to pursue this as a point-of-care option. Given the scale of this combinatorial chip, further study into increasing the shelf-life of molecular beacons and storage conditions to maintain fidelity of the beacon operation. Also, expanding the chip to include a larger combination of screens with increased combinations would be an impressive benefit for large scale combinatorics and screening techniques of patient samples. If the molecular beacon work could be expanded to include fluorescence-based sensitivity to the presence of mutants, it is expected that these microfluidic chips could achieve a higher sensitivity using fewer amounts of molecular beacons to viruses and virus mutants. In the current

state, additional work is needed to determine if the fluorescence signal is strong enough at the microscale for these combinatorial screening systems.

4.4. Materials and Methods

4.4.1. Device Fabrication

Devices were prepared in Freehand MX using multilayer soft lithography as discussed in previous work [37, 38]. For designing the combinatorial screening chip, the fluid layer was composed of a network of four horizontal channels intersecting with four vertical channels, each 75 μm in width. At the end of these channels, 600 μm circular regions were designed to make the inlet/outlet ports. The half-well chambers were composed of 250 μm circles connected to 150 μm lines forming the U-shaped half-wells. All gaps for these microchannels were 40 μm in width and placed at an angle whenever possible to reduce the pressure required to open the valves.

The control layer was also designed using Freehand MX. Square valves were placed throughout the device to cover each gap of the fluid layer, measuring 248 μm x 236 μm for the valves over horizontal flowing microchannels, 198 μm x 495 μm for the valves over the vertical flowing channels, and 292 μm x 347 μm for the mixing valves. These valves were connected via 49 μm microchannel runner lines to three input circles, 600 μm in diameter. In order to connect the three types of valves to only three valve inputs, the mixing and the vertical movement valves were interdigitated across the chip, with the horizontal flowing valves snaking back and forth throughout the design. Because the horizontal valves travel across the farthest length, these valves were the

most susceptible to vacuum leakage and were often the first to malfunction if the chip showed signs of failure.

These designs were then replicated onto a transparency mask using the laser printing services of the University of Illinois Print Shop. Two silicon wafers were first cleaned using acetone and then isopropanol, followed by drying under nitrogen and heated to 110°C to remove any water that might condensate onto the silicon wafers during drying for 10 minutes. At the end of this drying time, the wafers were placed inside a spin coater. Two milliliters of SU-8 25 were placed on the center of the wafer for spin coating treatment. The program run by the spin coater ramped up to 2000 RPMs over 10 seconds, and then held at 2000 RPMs for 30 additional seconds. After this, it ramped back down to 0 RPMs in 10 seconds. This procedure yielded a thin layer of photoresist 25 μm in height.

After coating, the wafer was then placed onto a hot plate preset at 65°C for 4 minutes. The wafer was then transferred to the second hot plate at 95°C for 8 minutes. The wafer was then allowed to cool for 1 minute, and then placed in a collimated UV light source and exposed for 20 seconds at 11 $\mu W/cm^2$. The wafer was then developed in PGMEA (propylene glycol methyl ether acetate) for 5 minutes, taking care to rinse with ispropanol. If any white residue remained on the surface of the silicon wafer, it was placed back in the PGMEA and developed further. When the silicon wafer could be rinsed with isopropanol and no white residue remained, the wafer was subsequently dried under nitrogen and stored in a petri dish. At this point, the silicon wafers with photoresist designs are called masters.

To prepare these masters for device production, they were first placed in a dessicator with silanizing agent for four hours. PDMS base and crosslinking agents were mixed in a 5:1 ratio for the control layer, and a 15:1 ratio for the fluid layer. This difference in crosslinker ratio allows for a tighter bond between the two layers after partially curing the layers separately. The very first time a control master is used for device fabrication, 30 g of PDMS mixture will be required to pour into a standard size petri dish, which will yield a device with a thickness around 3-5 mm. Subsequent devices made with the control master will only need 15 g of PDMS, due to the ring of unused PDMS that can be used as a placeholder from earlier device fabrication attempts. For the fluid layer, only 10 g of PDMS mixture is needed. 1-2 mL of PDMS is poured onto the surface of a fluid layer master, which is then placed inside a spin coater for the same program outlined above at 2000 RPMs. This will yield a thickness of 45 μm PDMS for microchannels that are 25 μm in height.

Both layers are placed inside an oven set to 65°C for 30 minutes, and are then checked for tackiness. If the PDMS on the fluid layer master is solid but still sticky, the device can be aligned. The control layer is cut out using a razor or scalpel, and holes are punched to connect to the valves in the control layer. Given that the height of the control channels are only 25 μm, this pattern can be very challenging to see. The use of additional and direct lighting is absolutely required, since any failed punch will destroy the utility of the device. When all holes to the control layer valves have been punched, the fluid layer master is placed onto a vacuum-chuck mount under a microscope. Alignment requires careful placement of the control layer above the fluid layer, while

making sure valves align properly to gaps in the fluid layer. This can be done by hand, or using a mechanical alignment system for careful iterative adjustment. If only a certain portion of the valves are aligned, the device can be lifted at a corner, causing the design to be stretched or contorted to fit all valves onto the fluid layer.

Once the valves are aligned, the device is placed into the oven at 65°C for 1 hour to fully cure the layers together to form an irreversible seal. After curing, the device is cut from the fluid layer master using a scalpel or razor, and holes are punched to provide inlets for the fluid layer microchannels exposed on the bottom of the device. If the device is not to be used immediately in an experiment, it is placed onto a pre-cleaned glass slide to ensure that no dust particles adhere to the clean microchannel surface underneath.

4.4.2. Solution Preparation

All DNA materials are ordered lyophilized from Integrated DNA Technologies. Upon receipt of the molecular beacon or oligonucleotide samples, the sample is dissolved in TE 50 buffer (10 mM Tris/HCl buffer [pH = 8.0], 1 mM EDTA, 50 mM NaCl) to a concentration of 100 or 200 μM. These stock solutions are stored in a -20°C freezer for long term storage. Neutravidin and BSA-Biotin are purchased lyophilized from Sigma Aldrich. These 1g pellets are dissolved in TE 50 buffer, and freeze dried in liquid nitrogen in 50 μL aliquots at a concentration of 5g/mL and 10 g/mL respectively. These aliquots are stored in a -80°C freezer. Before each experiment, an aliquot each of the Neutravidin and BSA-biotin tubes are removed from the freezer and thawed by hand, followed by the addition of 450 μL of TE 50 buffer. For the surface chemistry protocol,

the final concentrations of the BSA-biotin and Neutravidin aliquots are 1.0 g/mL and 0.5 g/mL, respectively.

4.4.3. Surface Chemistry Protocol

For all experiments, a glass slide was cleaned with acetone, isopropyl alcohol and millipore water. The slide was then dried under argon, and either built into a glass flow cell or integrated to a PDMS-based microfluidic screening chip. BSA-biotin (1 mg/mL) in TE 50 buffer was loaded for 15 minutes into the microchannels of the device. These were then rinsed with TE 50 buffer. Neutravidin (0.5 mg/mL) in TE 50 buffer was loaded for 15 minutes into the microchannels of the device and subsequently rinsed with TE 50 buffer. Molecular beacons, in concentrations varying from 100 pM to 250 nM, were introduced into the chip and allowed to incubate between 15 and 60 minutes, depending on the experiment. After loading, extra beacons were rinsed out with TE 50 buffer or imaging buffer.

4.4.4. Glass flow cells

Glass slides were cleaned using acetone, isopropanol and millipore water. They were then dried under nitrogen. Double sided tape was placed on one glass slide, with excess tape cut off with a razor. The second glass slide was then mounted on top of the tape, creating an open microchannel in a glass-based flow cell.

4.4.5. Microscope Setup

The fluorescence microscope used a green laser (538 nm, 625 μW) focused to the back of a 100x objective on an inverted microscope. The focal point of an incoming

lens was adjusted to focus the beam at the incident angle in the microfluidic device/flow cell. After passing through a filter, fluorescence was taken on an Andor Solis camera. Data collection was done for 500 millisecond intervals for a kinetic run between 20 and 100 pictures. Three spots were taken over the 20 or 100 picture kinetic length, and all pictures were averaged together over a region of interest centered on the Gaussian excitation beam.

4.4.6. Multiplex Screening Experiment

For the combinatorial multiplex screening experiment, the devices were assembled as above in Section 4.4.1. After the device is finished, it is mounted onto a cleaned glass coverslip and treated to the surface chemistry steps in Section 4.4.3. For the multiplex screening experiment, four different molecular beacons were introduced within each row of the combinatorial screening chip at a concentration of 250 μM. These beacons were allowed to incubate for 30 minutes, and subsequently rinsed with TE 50 buffer. The device and coverslip were then mounted onto the fluorescence microscope outlined in Section 4.4.5. Within each well with rinsed beacons, three regions of interest were identified within the confines of the horizontal half-wells using brightfield illumination. Just before data collection, the shutter for the excitation laser was opened, impinging on combinatorial device at the incident angle in TIRF. 100 images (500 msec exposure) were taken, recording an absolute value of the fluorescence collection on an Andor Solis camera.

At the conclusion of the last image, the file was saved as a stack in TIFF format. After all wells had three regions of interest studied, the device was then transported to a

microscope and the subsequent target oligonucleotides were introduced into the vertical chambers, using the vertical valve operation under vacuum [39]. After all four target oligonucleotides were introduced into the vertical half-wells, the mixing valve was opened and closed over 30 minutes to force the oligonucleotide solutions to mix across each of the surfaces with specifically linked molecular beacons in a combinatorial, but discrete fashion. The valves remained open for 30 minutes after this.

The valves were then allowed to relax back to rest state, isolating all half-wells throughout the device. The device was then transported back to the fluorescence microscope, and half-well chambers were once again located in brightfield lumination. Within each well, three new regions of interest were located away from previously identified regions of interest. For each of these new regions of interest, fluorescence was collected by the camera for 100 images.

For analysis, the averaged values of the spots were performed using ImageJ across a selected region on all stacks, and these final values were averaged to determine the count value for a particular well. When plotting the average value of a stack over each of the images within that stack (a function of time), the fluorescence detection was observed to generally decrease as a function a time, a result of the photobleaching occurring during this experiment.

4.4.7. Multiplex Screening Experiment with Imaging Buffer

As a method to discourage photobleaching and introduce lower concentrations of molecular beacons, an oxygen scavenger was used in the buffer to reduce the amount

of photobleaching during the experiment. 2% wt/v glucose oxidase, 2% wt/v catalase and 0.04 % wt/v glucose were dissolved in TE 50 buffer and used for the imaging buffer.

For these experiments, surface chemistry treatment remained the same. However, four different molecular beacons at concentrations of 100 pM were loaded for 15 minutes in order to reduce the amount of beacon loading on the surface. After these beacons were loaded, the remaining solution was rinsed out using imaging buffer. At these concentrations, the oxygen scavenger in the imaging buffer no longer functions after 1 hour has passed. To accommodate this, the four target oligonucleotides were introduced into the vertical half-wells all on chip. Three regions of interest were selected within each well, but was limited to 20 pictures because of time constraints. After all pictures were taken, the device was transported to a microscope and mixing valves were activated by vacuum. Oligonucleotides were allowed 20 minutes to mix and hybridize to the molecular beacons. The device was then transported back to the fluorescence microscope and fluorescence data was again collected in the same fashion. The image analysis protocol remained the same.

4.5. References

1. Proudnikov, D. and A. Mirzabekov, *Chemical methods of DNA and RNA fluorescent labeling.* Nucleic Acid Res., 1996. **15**(24(22)): p. 4535-4542.
2. Abd El Galil, K.H., M.A. El Sokkary, S.M. Kheira, A.M. Salazar, M.V. Yates, W. Chen, and A. Mulchandani, *Combined Immunomagnetic Separation-Molecular Beacon-Reverse Transcription-PCR Assay for Detection of Hepatitis A Virus from Environmental Samples.* Appl. Environ. Microbiol., 2004. **70**(7): p. 4371-4374.
3. Marras, S.A.E., F. Russell Kramer, and S. Tyagi, *Multiplex detection of single-nucleotide variations using molecular beacons.* Genetic Analysis: Biomolecular Engineering, 1999. **14**(5-6): p. 151-156.
4. Tyagi, S. and F.R. Kramer, *Molecular Beacons: Probes that Fluoresce upon Hybridization.* Nat Biotech, 1996. **14**(3): p. 303-308.
5. Vet, J.A.M., A.R. Majithia, S.A.E. Marras, S. Tyagi, S. Dube, B.J. Poiesz, and F.R. Kramer, *Multiplex detection of four pathogenic retroviruses using molecular beacons.* Proceedings of the National Academy of Sciences of the United States of America, 1999. **96**(11): p. 6394-6399.
6. Tyagi, S. and F.R. Kramer, *Molecular Beacons: Probes that Fluoresce upon Hybridization.* Nature Biotechnology, 1995. **14**(March 1996): p. 303-308.
7. Lewin, S.R., M. Vesanen, L. Kostrikis, A. Hurley, M. Duran, L. Zhang, D.D. Ho, and M. Markowitz, *Use of Real-Time PCR and Molecular Beacons to Detect Virus Replication in Human Immunodeficiency virus Type 1-Infected Individuals on Prolonged Effective Antiretrovial Therapy.* J. Virol., 1999. **73**(7): p. 6099-6103.
8. Thompson, N.L., T.P. Burghardt, and D. Axelrod, *Measuring surface dynamics of biomolecules by total internal reflection fluorescence with photobleaching recovery or correlation spectroscopy.* Biophysical Journal, 1981. **33**: p. 435-454.
9. Axelrod, D., *Cell substrate contacts illuminated by total internal reflection fluorescence.* J Cell Biol, 1981. **89**: p. 141-145.
10. Stout, A.L. and D. Axelrod, *Evanescent field excitation of fluorescence by epi-illumination microscopy.* Applied Optics, 1989. **28**(24): p. 5237-5242.
11. White, J.G., W.B. Amos, and M. Fordham, *An evaluation of confocal versus conventional imaging of biological structures by fluorescence light microscopy.* J Cell Biol, 1987. **105**: p. 41-48.
12. Ruckstuhl, T. and S. Seegar, *Attoliter detection volumes by confocal total-internal-reflection fluorescence microscopy.* Opt Lett, 2004. **29**: p. 569-571.
13. Prober, J., G. Trainor, R. Dam, F. Hobbs, C. Robertson, R. Zagursky, A. Cocuzza, M. Jensen, and K. Baumeister, *A system for rapid DNA sequencing*

with fluorescent chain-terminating dideoxynucleotides. Science, 1987. **238**(4825): p. 336-341.

14. Moyzis, R.K., J.M. Buckingham, L.S. Cram, M. Dani, L.L. Deaven, M.D. Jones, J. Meyne, R.L. Ratliff, and J.R. Wu, *A highly conserved repetitive DNA sequence, (TTAGGG)n, present at the telomeres of human chromosomes.* Proceedings of the National Academy of Sciences of the United States of America, 1988. **85**(18): p. 6622-6626.
15. Zhu, Z., J. Chao, H. Yu, and A.S. Waggoner, *Directly labeled DNA probes using fluorescent nucleotides with different length linkers.* Nucl. Acids Res., 1994. **22**(16): p. 3418-3422.
16. Ramsay, G., *DNA chips: State-of-the art.* Nat Biotech, 1998. **16**(1): p. 40-44.
17. Rayburn, A.L. and B.S. Gill, *Use of biotin-labeled probes to map specific DNA sequences on wheat chromosomes.* J Hered, 1985. **76**(2): p. 78-81.
18. Patolsky, F., A. Lichtenstein, and I. Willner, *Amplified Microgravimetric Quartz-Crystal-Microbalance Assay of DNA Using Oligonucleotide-Functionalized Liposomes or Biotinylated Liposomes.* Journal of the American Chemical Society, 1999. **122**(2): p. 418-419.
19. Song, J., C. Midson, E. Blachly-Dyson, M. Forte, and M. Colombini, *The Topology of VDAC as Probed by Biotin Modification.* Journal of Biological Chemistry, 1998. **273**(38): p. 24406-24413.
20. Heitzmann, H. and F.M. Richards, *Use of the Avidin-Biotin Complex for Specific Staining of Biological Membranes in Electron Microscopy.* Proceedings of the National Academy of Sciences of the United States of America, 1974. **71**(9): p. 3537-3541.
21. Pantano, P. and W.G. Kuhr, *Dehydrogenase-modified carbon-fiber microelectrodes for the measurement of neurotransmitter dynamics. 2. Covalent modification utilizing avidin-biotin technology.* Analytical Chemistry, 1993. **65**(5): p. 623-630.
22. Weinstock, R., R. Sweet, M. Weiss, H. Cedar, and R. Axel, *Intragenic DNA spacers interrupt the ovalbumin gene.* Proceedings of the National Academy of Sciences of the United States of America, 1978. **75**(3): p. 1299-1303.
23. Jensen, M.A., J.A. Webster, and N. Straus, *Rapid identification of bacteria on the basis of polymerase chain reaction-amplified ribosomal DNA spacer polymorphisms.* Appl. Environ. Microbiol., 1993. **59**(4): p. 945-952.
24. Saghai-Maroof, M.A., K.M. Soliman, R.A. Jorgensen, and R.W. Allard, *Ribosomal DNA spacer-length polymorphisms in barley: Mendelian inheritance, chromosomal location, and population dynamics.* Proceedings of the National Academy of Sciences, 1984. **81**: p. 8014-8018.

25. Baldwin, B.G., *Phylogenetic Utility of the Internal Transcribed Spacers of Nuclear Robosomal DNA in Plants: An example from the Comositae.* Molecular Phyologenetics and Evolution, 1992. **1**(1): p. 3-16.

26. Hendrickson, W.A., A. Pahler, J.L. Smith, Y. Satow, and E.A. Merrit, *Crystal structure of core streptavidin determined from multiwavelength anomalous diffraction of synchrotron radiation.* Proceedings of the National Academy of Sciences, 1989. **86**(7): p. 2190-2194.

27. O'Neill, M., D.T. Dryden, and N.E. Murray, *Localization of a protein-DNA interface by random mutagenesis.* EMBO J, 1998. **17**(23): p. 7118-7127.

28. Moreira, B.G., Y. You, M.A. Behlke, and R. Owczarzy, *Effects of fluorescent dyes, quenchers, and dangling ends on DNA duplex stability.* Biochemical and Biophysical Research Communications, 2005. **327**(2): p. 473-484.

29. Tyagi, S. and F. Kramer, Nature Biomolecular Engineering, 1996. **14**(303-308).

30. Takacs, T., C. Jeney, L. Kovacs, J. Mozes, M. Benczik, and A. Sebe, *Molecular beacon-based real-time PCR method for detection of 15 high-risk and 5 low-risk HPV types.* Journal of Virological Methods, 2008. **149**: p. 153-162.

31. Lewin, S.R., M. Vesanen, L. Kostrikis, A. Hurley, M. Duran, L. Zhang, D.D. Ho, and M. Markowitz, *Use of Real-Time PCR and Molecular Beacons To Detect Virus Replication in Human Immunodeficiency Virus Type 1-Infected Individuals on Prolonged Effective Antiretroviral Therapy.* J. Virol., 1999. **73**(7): p. 6099-6103.

32. Pas, S.D., S. Noppornpanth, A.A.v.d. Eijk, R.A.d. Man, and H.G. M. Niesters, *Quantification of the newly detected lamivudine resistant YSDD variants of Hepatitis B virus using molecular beacons.* Journal of Clinical Virology, 2005. **32**(2): p. 166-172.

33. McCahon, D., *The genetics of aphthovirus.* Archives of Virology, 1981. **69**(1): p. 0304-8608.

34. Jenkins, T.M., A.B. Hickman, F. Dyda, R. Ghirlando, D.R. Davies, and R. Craigie, *Catalytic domain of human immunodeficiency virus type 1 integrase: identification of a soluble mutant by systematic replacement of hydrophobic residues.* Proceedings of the National Academy of Sciences of the United States of America, 1995. **92**(13): p. 6057-6061.

35. Desrosiers, R.C., J.D. Lifson, J.S. Gibbs, S.C. Czajak, A.Y.M. Howe, L.O. Arthur, and R.P. Johnson, *Identification of Highly Attenuated Mutants of Simian Immunodeficiency Virus.* J. Virol., 1998. **72**(2): p. 1431-1437.

36. Miller, C.S., *Pleiotropic mechanisms of virus survival and persistence.* Oral Surgery, Oral Medicine, Oral Pathology, Oral Radiology, and Endodontology, 2005. **100**(2, Supplement 1): p. S27-S36.

37. Unger, M.A., H.-P. Chou, T. Thorsen, A. Scherer, and S.R. Quake, *Monolithic Microfabricated Valves and Pumps by Multilayer Soft Lithography.* Science, 2000. **288**(5463): p. 113-116.

38. Thorsen, T., S.J. Maerkl, and S.R. Quake, *Monolithic Microfabricated Valves and Pumps by Multilayer Soft Lithography.* Science, 2002. **298**: p. 580-584.

39. Schudel, B.R., C.J. Choi, B.T. Cunningham, and P.J.A. Kenis, *Microfluidic chip for combinatorial mixing and screening of assays.* Lab on a Chip, 2009. **9**: p. 1676.

Chapter 5

Conclusions and Future Directions

5.1. Conclusions

Screening can be a time-consuming process when hundreds or thousands of experiments need to be performed, but these experiments can be performed at the microscale using less reagents [1-4]. As observed in these studies, by downscaling the experiments, we can repeat experiments at the benchtop scale with the same accuracy and using far less reagent. Techniques such as multilayer soft lithography [5-8] also allow for smaller 'well plates' to be created afford a greater degree of control over the experiment and screening processes. Such microscale approaches can provide for a framework for a higher degree of complexity at these small scales. The microfluidic screening components presented here not only exploit, but also depend upon the physical characteristics of the microscale in order to operate.

As deduced in the design rules discovered for valve operation, there is a strong affinity between the PDMS and glass. In fact, valve failure is almost entirely influenced by the strong adhesive forces between these two materials. Valve actuation behavior could be tuned, either by changing parameters such as microchannel width or geometry to change the opening pressure, or by changing the thickness of the PDMS layer to change the closing pressure of the device. In chapter 2 these valves were observed to be dependent on the width of the fluidic microchannel, which could change the pressure

requirements by as much as 100-200 torr. By increasing the thickness of the fluid channel thickness, the valves were less likely to open, due to the increase in membrane stiffness. When the geometry of the valves was changed, weak points were introduced on the chip, which reduced the required pressure to separate the PDMS from the glass surface needed to operate the valve. These experiments provided a deeper understanding of the factors that determine valve operation and from this design rules were derived to aid the development of high density systems that are required for high throughput screening processes.

In Chapter 3, the AtO valves designed and studied in chapter 2 were employed in a combinatorial screening chip. At the microscale, surface to volume ratios are typically high, and this ratio was exploited using a surface-based approach to sensing the combinatorial reactions performed on chip. For sensing purposes, the combinatorial chip was integrated with a patterned photonic crystal biosensor, which identified changes in binding within each half-well of a 4 x 4 combinatorial mixing chip [9]. Sixteen compartments, controlled by three separate valves, were designed at a reaction density of 1/mm^2 for all fill lines and valves. Within these very small densities, the valves coordinate filling in the horizontal direction, the vertical direction and mixing. For a given half-well, 200 pL of reactant A can mix with 200 pL of reactant B, and this can be done all in concert to provide A_1B_1 to A_4B_4 products. This chip was validated with a proof-of-principle protein-antibody assay, demonstrating the combinatorial mixing capabilities of the chip.

For DNA-based sensing of viruses, the combinatorial mixing chip was employed with surface-bound molecular beacons as described in Chapter 4. The combinatorial nature of the microfluidic chip developed in Chapter 3 was employed with little alteration for this purpose. Since the device uses AtO valves with a reversible seal, the bottom layer of the device was interchanged from the photonic crystal biosensor to a molecular beacon patterned cover slip. These molecular beacons were observed to have a high background in glass-based flow cell studies, which was overcome by employing analysis using TIRF microscopy in which only the area just above the surface was excited. The 4x4 combinatorial chip tested four molecular beacons against four different virus-representative oligomer samples from conserved regions within the genes of each virus [10-13]. The surface-based approach of this analysis coupled to the microscopy technique of TIR meant that these studies could be performed using 100 pM of molecular beacon samples at very small volumes, orders of magnitude less than previously published sensitivity studies [14, 15].

In both screening techniques, the physics of the microscale was exploited to duplicate bench scale experiments at the microscale, using far less material while maintaining the fidelity of the results. For drug discovery, this would reduce the amount of potentially precious reagent used for testing against disease-related proteins. For virus detection, the combinatorial chip can exploit the surface-based approach of mounted molecular beacons and TIRF to discover the presence of a particular DNA sequence. These results were validated against what was expected at larger scales, but both were performed with far less reagent than what was used in the literature.

5.2. Future Directions

The next step for this work in microfluidic screening would be to apply the system to real-world problems, tackling the next set of variables that arise with more complex biological systems.

The design rules elucidated in Chapter 2 for the actuate-to-open valves provide a greater framework for future microfluidic devices. With this knowledge, the devices made here could be scaled out with a greater confidence of operation. A typical problem in valve actuation lies in the gas permeability of PDMS. As control channel lines become longer and longer over a large array of reaction sites, the pressure drop becomes more and more significant. With these design rules derived in this work, it is now easier to scale these devices out to create large arrays typical of 8 x 12 microplates studies used in conventional screening studies.

One future direction for the valves would be in new materials. The valves presented here are fabricated using PDMS, which is an elastomeric polymer that is incompatible with many organic solvents. PDMS is an ideal polymer for research purposes. Small changes in device design can be made within a few days. Unfortunately, this attractive rapid device development characteristic comes with issues such as poor shelf life and the aforementioned solvent incompatibility. For the medical devices discussed above, fluidic routes can be studied using PDMS-based chips, but for something that would need to survive on a shelf in a hospital for months at a time, a new polymer must be developed. Being able to fabricate these valves in a more solvent-compatible polymer would open up a vast array of possible chemical synthesis routes and applications.

The screening experiments performed using the photonic crystal biosensor were validated with a proof-of-principle experiment, but other routes exist for this kind of integrated chip. The protein-antibody experiment was good for demonstrative purposes, and now that the fluidics are established and validated at the microscale, the new frontier would be to examine new protein - combinatorial library interactions. Previous work in click chemistry has yielded several small molecule libraries of heterocyclic compounds made with precious reagent with well studied examples of interactions with cancer-related proteins. Validating that screen at the microscale would be another big step forward in advancing high throughput combinatorial technology for drug discovery.

The next steps for the multiplex virus identification chip would include working with actual viruses to determine how other biological components might contribute to fouling of the surface-beacon controlled surface. In microplate studies, molecular beacons were able to discover virus quantities as low as 1 active virus unit using epifluorescence microscopy. Validating these same results at the microscale using real components such as human blood would advance the field of diagnostics. Reducing the identification threshold could lead to hospital-based diagnostic studies that use very small amounts of blood to achieve accurate results in point-of-care tests. This kind of patient care advancement is constantly sought after for microscale-based devices.

5.3. References

1. Verpoorte, E., Electrophoresis, 2002. **23**: p. 677-712.

2. Schulte, T.H., R.L. Bardell, and B.H. Weigl, Clinica Chimca Acta, 2002. **321**: p. 1-10.

3. Zhong, J.F., Y. Chen, J.S. Marcus, A. Scherer, S.R. Quake, C.R. Taylor, and L.P. Weiner, Lab on a Chip, 2007. **8**: p. 68-74.

4. Dittrich, P.S. and A. Manz, Nature Reviews Drug Discovery, 2006. **5**: p. 210-218.

5. Unger, M.A., H.-P. Chou, T. Thorsen, A. Scherer, and S.R. Quake, *Monolithic microfabricated valves and pumps by multilayer soft lithography.* Science, 2000. **288**: p. 113-116.

6. Thorsen, T., S.J. Maerkl, and S.R. Quake, *Monolithic Microfabricated Valves and Pumps by Multilayer Soft Lithography.* Science, 2002. **298**: p. 580-584.

7. Grover, W.H., A.M. Skelley, C.N. Liu, E.T. Lagally, and R.A. Mathies, *Monolithic membrane valves and diaphragm pumps for practical large-scale integration into glass microfluidic devices.* Sensors and Actuators B: Chemical, 2003. **89**(3): p. 315-323.

8. Grover, W.H., R.H.C. Ivester, E.C. Jensen, and R.A. Mathies, *Development of multiplexed control of latching pneumatic valves using microfluidic logical structures.* Lab on a Chip, 2006. **6**: p. 623-631.

9. Schudel, B.R., C.J. Choi, B.T. Cunningham, and P.J.A. Kenis, *Microfluidi chip for combinatorial mixing and screening of assays.* Lab on a Chip, 2009. **accepted**.

10. Abd El Galil, K.H., M.A. El Sokkary, S.M. Kheira, A.M. Salazar, M.V. Yates, W. Chen, and A. Mulchandani, *Combined Immunomagnetic Separation-Molecular Beacon-Reverse Transcription-PCR Assay for Detection of Hepatitis A Virus from Environmental Samples.* Appl. Environ. Microbiol., 2004. **70**(7): p. 4371-4374.

11. Pas, S.D., S. Noppornpanth, A.A.v.d. Eijk, R.A.d. Man, and H.G. M. Niesters, *Quantification of the newly detected lamivudine resistant YSDD variants of Hepatitis B virus using molecular beacons.* Journal of Clinical Virology, 2005. **32**(2): p. 166-172.

12. Lewin, S.R., M. Vesanen, L. Kostrikis, A. Hurley, M. Duran, L. Zhang, D.D. Ho, and M. Markowitz, *Use of Real-Time PCR and Molecular Beacons to Detect Virus Replication in Human Immunodeficiency virus Type 1-Infected Individuals on Prolonged Effective Antiretrovial Therapy.* J. Virol., 1999. **73**(7): p. 6099-6103.

13. Takacs, T., C. Jeney, L. Kovacs, J. Mozes, M. Benczik, and A. Sebe, *Molecular beacon-based real-time PCR method for detection of 15 high-risk and 5 low-risk HPV types.* Journal of Virological Methods, 2008. **149**: p. 153-162.

14. Lewin, S.R., M. Vesanen, L. Kostrikis, A. Hurley, M. Duran, L. Zhang, D.D. Ho, and M. Markowitz, *Use of Real-Time PCR and Molecular Beacons To Detect Virus Replication in Human Immunodeficiency Virus Type 1-Infected Individuals on Prolonged Effective Antiretroviral Therapy.* J. Virol., 1999. **73**(7): p. 6099-6103.

15. Vet, J.A.M., A.R. Majithia, S.A.E. Marras, S. Tyagi, S. Dube, B.J. Poiesz, and F.R. Kramer, *Multiplex detection of four pathogenic retroviruses using molecular beacons.* Proceedings of the National Academy of Sciences of the United States of America, 1999. **96**(11): p. 6394-6399.